remote sensing

MDPI

Article

Joint Detection, Tracking, and Classification of Multiple Extended Objects Based on the JDTC-PMBM-GGIW Filter

Yuansheng Li [1], Ping Wei [1], Mingyi You [2], Yifan Wei [1] and Huaguo Zhang [1,*]

[1] School of Information and Communication Engineering, University of Electronic Science and Technology of China, Chengdu 611731, China
[2] Science and Technology on Communication Information Security Control Laboratory, Jiaxing 314033, China
* Correspondence: uestczhanghuaguo@uestc.edu.cn

Abstract: This paper focuses on the problem of joint detection, tracking, and classification (JDTC) for multiple extended objects (EOs) within a Poisson multi-Bernoulli (MB) mixture (PMBM) filter, where an EO is described as an ellipse, and the ellipse is modeled by a random matrix. The EOs are classified according to the size information of the ellipse. Usually, detection, tracking, and classification are processed step-by-step. However, step-by-step processing ignores the coupling relationship between detection, tracking, and classification, resulting in information loss. In fact, detection, tracking, and classification affect each other, and JDTC is expected to be beneficial for achieving better overall performance. In the multi-target tracking problem based on RFS, the overall performance of the PMBM filter satisfying the conjugate priors has been verified to be superior to other filters. Specifically, the PMBM filter propagates multiple MB simultaneously during iterative updates and model the distribution of hitherto undetected EOs. At present, the PMBM filter is only applied to multiple extended objects tracking problem. Therefore, we consider using the PMBM filter to solve the JDTC problem of multiple EOs and further improve JDTC performance. Furthermore, the closed-form implementation based on the product of a gamma Gaussian inverse Wishart (GGIW) and class probability mass function (PMF) is proposed. The details of parameters calculation in the implementation process and the derivation of class PMF are presented in this paper. Simulation experiments verify that the proposed algorithm, named the JDTC-PMBM-GGIW filter, performs well in comparison to the existing JDTC strategies for multiple extended objects.

Keywords: joint detection, tracking and classification; random matrix; gamma Gaussian inverse Wishart; extended objects

Citation: Li, Y.; Wei, P.; You, M.; Wei, Y.; Zhang, H. Joint Detection, Tracking, and Classification of Multiple Extended Objects Based on the JDTC-PMBM-GGIW Filter. *Remote Sens.* **2023**, *15*, 887. https://doi.org/10.3390/rs15040887

Academic Editor: Qi Wang

Received: 28 December 2022
Revised: 31 January 2023
Accepted: 2 February 2023
Published: 5 February 2023

1. Introduction

Multiple target tracking is an important technique in many fields [1–15]. Traditionally, an object can be modeled as a point object if it is detected, and at most one sensor resolution cell is occupied by the object. In this case, each object gives rise to at most a single measurement per time frame/scan [1–12]. In reference [1], a data association solution suitable for multiple objects tracking is proposed, which can effectively track pedestrians in thermal images. To solve the data association problems in thermal images, they create a hybrid data association function that fuses data-driven scores and feature engineering scores to obtain a high-quality and adaptable tracking method. However, this approach relies excessively on a dataset created from thermal images in the process of training data-driven models to learn features. Due to the multipath propagation effects when tracking low altitude target, the measured elevation angle of the target degrades seriously. To solve this problem, Reference [3] proposed a tracking algorithm to alleviate the influence of multipath. Although this method does not require an elaborate model with physical parameters of the propagation phenomenology, its robustness still needs to be improved. For the merged measurement problem in multiple target tracking, Reference [4] proposed a JPDA-based

Bayesian filter, which provides improved model fidelity and takes into account the possibility that a measurement is derived from unresolved targets. However, the filter proposed in Reference [4] needs to deal with combinatorial problems, so the computational complexity increases rapidly with the number of targets. In recent years, due to rapid advances in sensor technology, it is becoming commonplace that an object occupies several sensor resolution cells. Tracking an object that may occupy more than one sensor cell is called extended objects tracking [5–13,16]. Compared to the traditional point target, the number of measurements that an EO can produce is uncertain. The measurements of EOs contain both the kinematic information and the extension information of the EO, such as scale, shape, direction, etc. In general, an EO measurement is described by the inhomogeneous Poisson Point Process (PPP) [5,17], i.e., the number of measurements is given by a Poisson distributed random number, and spatially, measurements are distributed around the EO. The Poisson distribution is characterized by the measurement rate (MR) of each EO [18]. Several models describing target extensions are exploited, such as the random matrix model [6,17] and the random hypersurface model [19], and the Gaussian process [20]. The random matrix model assumes that the measurements modeled by a Gaussian distribution are distributed around the centroid of the EO. For the EO tracking problem with arbitrary shapes, modeling EOs with a random hypersurface model or Gaussian process involves more parameter calculation. Although more accurate and detailed target contours can be obtained, this is usually at the cost of significantly increasing complexity. Recently, a mathematically tractable new analytical model was proposed in Reference [21], in which the EO is represented by its central position, the orientation (heading), and the perimeter contour. The model is rich enough to capture the backscattering effects of the EO shape, and the number of contour parameters of an EO is tractable. In order to estimate the kinematic state and extension of the EO with complex shape more flexibly and easily, Reference [22] developed an effective extension-deformation model for an EO tracking, in which the object extension is fully characterized by several deformed control points. The method, based on the extension-deformation model, needs to obtain the prior distribution information of the measurement sources by sampling. However, the tracking methods for irregular shape EO in References [21,22] are only for the scenario of a single EO. Since an EO may be associated with multiple measurements, the number of data associations in multiple EOs tracking grows exponentially with the number of EOs and measurements. It makes the multiple EOs tracking problem more challenging.

So far, multiple extended objects tracking based on the random finite set (RFS) framework has been continuously presented [2]. Mahler derived the measurement update expression of the probability hypothesis density (PHD) filter, which is used to track the Poisson modeling EOs [23,24]. Subsequently, an EO-PHD filter describing the target extension with a random matrix is presented [16,17]. In Reference [16], the method estimating the shape parameters of ellipse EO based on Kalman filter is integrated into GM-PHD filter, and the Minimum-Cost Flow (MCF) approach is adopted to label the trajectory of EOs. The method in Reference [16] can track multiple EOs efficiently and consistently, and improve the target trajectory estimation in specific scenarios. However, in this method, the ellipse EO is parameterized to the orientation and semi-axis length, so the measurement information received by the sensors cannot be used directly. In the updating process, additional pseudo-measurements need to be constructed, and the complex linearization processing is required. In Reference [25], the GM-PHD filter was generalized to track pedestrian groups. The method in Reference [25] has the ability to estimate the correct number of groups and accurately represent the size and shape of the groups. However, this method needs to convert the collected observation data in the frames from image coordinates to world coordinates in advance. In addition, the low detection probability implied by the image detection algorithm restricts the tracking performance of GM-PHD filter. Besides, an EO cardinalized probability hypothesis density (EO-CPHD) filter based EOs tracking is presented [26]. With gamma Gaussian inverse Wishart (GGIW) implementation, EO-CPHD can estimate the kinematic state, the extended state, and the Poisson measurement rate,

simultaneously. Later, the multi-Bernoulli (MB) filter [27,28], labeled multi-Bernoulli (LMB) and generalized LMB (GLMB) filters based EOs tracking have been proposed [12,14,29,30].

Recently, another type of RFS conjugate priors have been presented in the literature, i.e., the PMBM model [31,32], which consists of a Poisson process and a multi-Bernoulli mixture (MBM). The PMBM is a conjugate prior and it divides the target set into a detected target set and an undetected target set. The MBM considers all possible data association hypotheses for the detected targets. The PPP models all targets that have never been detected. Furthermore, the PMBM has been proven to have efficient computational performance [33]. The PMBM filtering recursions for extended objects tracking have already been explored in References [32,34]. In References [32,34], for the compared scenarios, the filters based on the PMBM conjugate prior generally outperform other RFSs-based filters, in terms of tracking performance and computational cost.

In order to ensure that the RFS-based JDTC algorithm not only satisfies the conjugate prior, but also improve the overall performance significantly, in this paper, we devote to generalizing the PMBM filter [32,34] to the JDTC problem with multiple EOs. We first augment the EO state to include class information, then, using prior size information related to the target class, PMBM for JDTC (JDTC-PMBM) filter recursion is established and class PMF of JDTC-PMBM density is derived. In order to implement the proposed JDTC-PMBM filter analytically and in a computationally feasible way, the product of a gamma Gaussian inverse Wishart (GGIW) distribution and class probability mass function (PMF) is adopted to approximately model the probability density of a single EO. The resulting algorithm, which is referred to as JDTC-PMBM-GGIW filter, can not only estimate the kinematic state, measurement rate, and extended state of the EOs, but also estimate the class probability of each EO. Further, the proposed JDTC-PMBM-GGIW method is evaluated in simulations, where its performance is compared to the existing RFS-based JDTC methods [35,36].

The main contributions of this paper are summarized as follows.

(1) The JDTC-PMBM filter recursion is proposed to perform JDTC of multiple EOs;
(2) The analytical and computationally feasible implementations of the proposed JDTC-PMBM filter are derived;
(3) The performance of the proposed approach is assessed via simulations.

2. Related Work

Joint detection, tracking, and classification (JDTC) of targets is a fundamental requirement of surveillance systems [15,37–45]. Specifically, the joint tracking and classification algorithm can not only estimate the kinematic characteristics of the target (such as target position, target extension, target velocity), but also identify the target according to the classification results, thus improving the tracking accuracy. The JDTC algorithm plays also an important role in threat assessment [15,38–45]. Usually, detection, tracking, and classification are processed step-by-step. However, step-by-step processing ignores the coupling relationship between detection, tracking, and classification, resulting in information loss. For EOs, detection, tracking, and classification are complementary. As a result, JDTC may improve the overall performance [35,46]. In Reference [44], the JDTC algorithms can be applied to accurately identify fighter aircraft types (such as F4 fighter, F15 fighter, and T38 fighter), providing more accurate information for the command and guidance system, so as to precisely strike the most threatening fighter aircraft.

The essence of JDTC of multiple ellipse extended objects is to estimate the posterior probability density of a target that has been classified and the class probability mass function (PMF) within a Bayesian framework, simultaneously. Therefore, the challenge of JDTC problem with multiple ellipse extended objects is how to integrate the prior scale information related to EO classes into the Bayesian framework. In Reference [46], it is proposed that the scale information related to EO classes is reasonably regarded as a pseudo-measurement and modeled as Wishart distribution. Through the modeling method of Reference [46], the JDTC problem of ellipse extended objects is analytically implemented by the Bayesian iterative updating process using the pseudo measurements

and the real measurements received by the sensors. Later, Reference [36] extended the ideas in Reference [46] to solve the JDTC problem of multiple ellipse extended objects. In Reference [36], the posterior density of multiple objects is modeled as PHD. Nevertheless, as is well known [2], the PHD filter has a problem of high cardinality variance and decreased performance with low detection probability and high clutter. In order to make up for the defects of the JDTC algorithm based on PHD filter (JDTC-GIW-PHD algorithm) [36], another JDTC algorithm of multiple extended objects based on RFS (JDTC-GIW-MeMBer algorithm) [35] and the JDTC algorithm of multiple extended objects based on message passing [41] are proposed successively. In Reference [35], the posterior density of multiple objects is modeled as a spatial probability density function of the MB parameter. In Reference [41], the posterior density of multiple objects is approximated by a belief function. However, neither the JDTC-GIW-PHD algorithm nor the JDTC-GIW-MeMBer algorithm satisfies the conjugate prior, and the JDTC-GIW-PHD algorithm and JDTC-GIW-MeMBer algorithm ignore the data association problem between EOs and measurements. In addition, the JDTC-GIW-MeMBer algorithm only propagates a single MB density.

In recent years, a PMBM density has been derived from the RFS frame. The PMBM density accurately approximates the EO's posterior density [31–34]. The PMBM filter not only satisfies conjugate a priori but also considers the data association between EOs and measurements. Different from the PHD filter and MeMBer filter, the PMBM filter models the detected targets through multiple MB mixture densities, so its tracking performance is significantly better than that of the PHD filter and MeMBe filter. In addition, since undetected targets are modeled by PPP, the PMBM filter can not only track the detected targets during occlusions, but also identify the surveillance areas where the undetected targets may exist [32]. To the best of the authors' knowledge, the JDTC problem for multiple EOs has not been explored in a PMBM filter yet.

3. Background

3.1. Dynamic Model

The state of each EO at time k is defined as $\mathbf{y}_k \triangleq [\xi_k^\top, \mathcal{C}_k^c]^\top$, specifically:

- $\xi_k = (\gamma_k, \mathbf{x}_k, \mathbf{X}_k)$, where $\mathbf{x}_k$, $\mathbf{X}_k$ represent the kinematic and extended states, respectively; γ_k denotes the Poisson measurement rate of such an EO.
- $\mathcal{C}_k^c \in \{\mathcal{C}_k^1, \mathcal{C}_k^2, \cdots, \mathcal{C}_k^{n_c}\}$ denotes the class state of an EO, n_c is the total number of categories for the EOs.

In this paper, the kinematic state $\mathbf{x}_k$ at time k is defined as $\mathbf{x}_k = (p_x^k, v_x^k, p_y^k, v_y^k)^\top$, it contains position and velocity information, and the state space dimension $d = 2$. $\mathbf{X}_k$ is the extended state of an EO, which is a symmetric positive define (SPD) random matrix.

The dynamic model of kinematic state $f(\mathbf{x}_k|\mathbf{x}_{k-1})$, extended state transitions in class state conditions $f(\mathbf{X}_k|\mathbf{x}_{k-1}, \mathbf{X}_{k-1}, \mathcal{C}_k^c)$ [7,46], and measurement rate transfer model [18] $f(\gamma_k|\gamma_{k-1})$ are described in detail in Reference [41]. In addition, we assume that the EO's class does not shift over time [35,36,46], i.e., $f(\mathcal{C}_k^c|\mathcal{C}_{k-1}^{c'}) = 1$ if $\mathcal{C}_k^c = \mathcal{C}_{k-1}^{c'}$ and otherwise $f(\mathcal{C}_k^c|\mathcal{C}_{k-1}^{c'}) = 0$.

3.2. The Measurement Analysis for JDTC

For the c-th class target, the extended matrix of the EO can be expressed as [36,46]

$$\mathbf{X}_k = (\mathbf{E}_k^c)^{-1} \mathbf{Z}_k^{p,c} (\mathbf{E}_k^c)^{-\top} \tag{1}$$

where $\mathbf{Z}_k^{p,c} \in \mathbb{R}^{d \times d}$ is a SPD matrix, which is given by

$$\mathbf{Z}_k^{p,c} = \mathrm{diag}(a_{p,c}^2, b_{p,c}^2) \tag{2}$$

where $a_{p,c}$ and $b_{p,c}$ are the major axis length and minor axis length of an ellipse, respectively. $\mathbf{E}_k^c$ is a matrix describing the direction of the ellipse, which is given by [36]

$$\mathbf{E}_k^c = \begin{bmatrix} \cos(\theta_k) & -\sin(\theta_k) \\ \sin(\theta_k) & \cos(\theta_k) \end{bmatrix} \tag{3}$$

where θ_k is the velocity direction.

The prior size matrix of the c-th class target $\mathbf{Z}_k^{p,c}$ is defined as a pseudo measurement. The pseudo measurement likelihood function is given by Reference [46]

$$\psi_{\mathbf{Z}_k^{p,c}}(\xi_k, \mathcal{C}_k^c) = \mathcal{W}(\mathbf{Z}_k^{p,c}; \delta_k^{p,c}, \mathbf{E}_k^c \mathbf{X}_k (\mathbf{E}_k^c)^\top / \delta_k^{p,c}) \tag{4}$$

where $\delta_k^{p,c}$ is the corresponding degree of freedom.

Suppose that the real measurement set of the EO is $\mathbf{C}_c$, and measurements in the measurement set are independent of each other. The spatial distribution of clutter measurement is $c(\mathbf{z})$ with the average number λ. The PPP intensity of clutter $\kappa(\mathbf{z}) = \lambda c(\mathbf{z})$. The detection probability of an EO is defined as $p_D(\xi_k, \mathcal{C}_k^c)$.

The real measurements originated by EOs are modeled as inhomogeneous Poisson point process (PPP) [5,17,32]. The likelihood function of the EO corresponding to the real measurements set $\mathbf{C}_c$ is given by

$$\begin{aligned} \psi_{\mathbf{C}_c}(\xi_k, \mathcal{C}_k^c) = {} & \mathcal{PS}(|\mathbf{C}_c|; \gamma_k(\xi_k, \mathcal{C}_k^c)) \cdot p_D(\xi_k, \mathcal{C}_k^c) \cdot e^{-\gamma_k(\xi_k, \mathcal{C}_k^c)} \\ & \times \prod_{\mathbf{z} \in \mathbf{C}_c} \gamma_k(\xi_k, \mathcal{C}_k^c) g(\mathbf{z}|\xi_k, \mathcal{C}_k^c) \end{aligned} \tag{5}$$

$$g(\mathbf{z}|\xi_k, \mathcal{C}_k^c) = \mathcal{N}(\mathbf{z}; \mathbf{H}_k \mathbf{x}_k, \mathbf{R}_k + \eta \mathbf{X}_k) \tag{6}$$

where $\mathbf{H}_k$ is the observation matrix, $\gamma_k(\xi_k, \mathcal{C}_k^c)$ is the Poisson measurement rate, the measurement spatial distribution is $g(\mathbf{z}|\xi_k, \mathcal{C}_k^c)$, $\mathbf{R}_k$ denotes the covariance of observation noise, η is a regulation parameter, $|\mathbf{C}_c|$ is the cardinality of measurements set $\mathbf{C}_c$, and $|\mathbf{C}_c|$ is assumed to follow a Poisson distribution [5,36].

The missed detection probability is given by

$$q_{\mathrm{D}}(\xi_k, \mathcal{C}_k^c) = 1 - p_{\mathrm{D}}(\xi_k, \mathcal{C}_k^c) + p_{\mathrm{D}}(\xi_k, \mathcal{C}_k^c) e^{-\gamma_k(\xi_k, \mathcal{C}_k^c)} \tag{7}$$

where $(1 - e^{-\gamma_k(\xi_k, \mathcal{C}_k^c)})$ is the probability that an EO produces at least a measurement. Define $q_{\mathrm{D}}(\xi_k, \mathcal{C}_k^c)$ as the likelihood function corresponding to the empty measurement set, i.e., $\psi_{\varnothing}(\xi_k, \mathcal{C}_k^c) = q_{\mathrm{D}}(\xi_k, \mathcal{C}_k^c)$ [32].

In addition, the measurement data satisfy the following assumptions:

1. Clutter is independent of the target-originated measurements and pseudo measurements;
2. The sensor has a linear Gaussian measurement model;
3. The measurements generated by each EO are independent of each other.

4. PMBM Filter for JDTC

4.1. Association Events

The real measurements set $\mathbf{Z}^{r,k}$ is given by

$$\mathbf{Z}^{r,k} = \{\mathbf{z}_m\}_{m \in \mathbb{M}} \tag{8}$$

For the targets of the j-th predicted global hypothesis, we define the j-th predicted global hypothesis index space as $\mathcal{A}^j$, and $A \in \mathcal{A}^j$ is an association. The measurements in $\mathbf{Z}^{r,k}$ are associated with an existing target indexed by $\mathbb{I}^j$ or a new target, or the measurements are generated by clutter. For all j, $\mathbb{M} \cap \mathbb{I}^j = \varnothing$. In fact, for the j-th predicted global hypothesis, a data association $A \in \mathcal{A}^j$ is a partition of $\mathbb{M} \cup \mathbb{I}^j$ into nonempty disjoint subsets $C \in A$, and the data associations space is described as $\mathcal{A}^j = \mathcal{P}(\mathbb{M} \cup \mathbb{I}^j)$. For multi-target tracking,

it is usually assumed that the measurements are independent of each other and that a measurement originates from at most one target, i.e., $|C \cap \mathbb{I}^j| \leq 1$ for all $C \in A$. If there are two or more target indices in the partitioned subset, the measurement likelihood is zero. If there is a target index in the subset C, the target index is defined as i_C. In addition, we group all the measurements in subset C into a measurement set named $\mathbf{C}_c$, i.e., $\mathbf{C}_c = \bigcup_{m \in C \cap \mathbb{M}} \mathbf{z}_m$.

4.2. PMBM Density for JDTC

The PMBM model [31–34] consists of a PPP and an MBM, where PPPs model the clutter, EO measurements, new EO, and undetected EOs, and the MBM is used to model the detected EO. For JDTC problems, the target state needs to be expanded to include class information. Thus, the intensity function of a PPP is given by $D^u(\xi_k, \mathcal{C}_k^c)$. An MBM density is a weighted sum of multiple MB densities. The weights are usually also the probabilities of different global hypotheses. An MBM is defined by parameters $\left\{\left(\mathcal{W}_k^j, \left\{\left(r_k^{j,i}, f^{j,i}(\xi_k, \mathcal{C}_k^c)\right)\right\}_{i \in \mathbb{I}^j}\right)\right\}_{j \in \mathbb{J}}$, where $r_k^{j,i}$ denotes the existence probability of each Bernoulli, $f^{j,i}(\cdot)$ is the spatial probability density function (PDF), $\mathbb{J}$ is an index space of the MBs in MBM, $\mathbb{I}^j$ is an index space of the Bernoullis in the j-th MB, $\mathcal{W}_k^j$ denotes the weight of the j-th MB. $|\mathbb{J}|$ is the number of MBs of MBM, $|\mathbb{I}^j|$ is the number of Bernoulli components in the j-th MB. In fact, each MB represents a global hypothesis about the detected EOs.

The set of the EOs state is defined as $\mathbf{Y}_k$, based on the PMBM model. $\mathbf{Y}_k$ can be divided into two disjoint subsets.

$$\mathbf{Y}_k^u, \mathbf{Y}_k^d : \mathbf{Y}_k^u \cup \mathbf{Y}_k^d = \mathbf{Y}_k, \mathbf{Y}_k^u \cap \mathbf{Y}_k^d = \varnothing \tag{9}$$

where $\mathbf{Y}_k^u$ and $\mathbf{Y}_k^d$ represent the set of detected EOs and the set of undetected EOs, respectively. The PMBM density for JDTC density is given by

$$f(\mathbf{Y}_k) = \sum_{\mathbf{Y}_k^u \uplus \mathbf{Y}_k^d = \mathbf{Y}_k} f^u(\mathbf{Y}_k^u) \sum_{j \in \mathbb{J}} \mathcal{W}^j f^j\left(\mathbf{Y}_k^d\right) \tag{10}$$

$$f^u(\mathbf{Y}_k^u) = e^{-\langle D^u; 1 \rangle} \prod_{\mathbf{y}_k \in \mathbf{Y}_k^u} D^u(\mathbf{y}_k) \tag{11}$$

$$f^j\left(\mathbf{Y}_k^d\right) = \sum_{\uplus_{i \in \mathbb{I}^j} \mathbf{Y}_k^i = \mathbf{Y}_k^d} \prod_{i \in \mathbb{I}^j} f_B^{j,i}(\mathbf{Y}_k^i) \tag{12}$$

where $f_B^{j,i}(\cdot)$ are the Bernoulli set densities, $\sum_{\uplus_{i \in \mathbb{I}}} \mathbf{Y}^i = \mathbf{Y}$ denotes a sum over all (possibly empty) subsets $\mathbf{Y}^i$, that are mutually disjoint, and whose union is $\mathbf{Y}$. $\langle \cdot, \cdot \rangle$ denotes the integral of the product of the two functions over all variables, i.e.,

$$\langle v; h \rangle = \sum_{\mathcal{C}_k^c} \iint_{\mathbf{x}_k, \mathbf{X}_k} v(\mathbf{x}_k, \mathbf{X}_k, \mathcal{C}_k^c) h(\mathbf{x}_k, \mathbf{X}_k, \mathcal{C}_k^c) d\mathbf{x}_k d\mathbf{X}_k \tag{13}$$

4.3. JDTC-PMBM Filter Recursion

The JDTC-PMBM density is described by the parameters

$$D^u(\mathbf{y}_k), \left\{\left(\mathcal{W}_k^j, \left\{(r_k^{j,i}, f^{j,i}(\mathbf{y}_k))\right\}_{i \in \mathbb{I}^j}\right)\right\}_{j \in \mathbb{J}} \tag{14}$$

The JDTC-PMBM filter recursion is presented as follows.

4.3.1. Prediction of JDTC-PMBM Filter

Given a posterior JDTC-PMBM density at time $k-1$ with parameters

$$D^u(\mathbf{y}_{k-1}), \left\{\left(\mathcal{W}_{k-1}^j, \left\{(r_{k-1}^{j,i}, f^{j,i}(\mathbf{y}_{k-1}))\right\}_{i \in \mathbb{I}^j}\right)\right\}_{j \in \mathbb{J}} \tag{15}$$

and the state transition model, the predicted JDTC-PMBM density is described by the parameters

$$D_+^u(\mathbf{y}_k), \left\{ \left(\mathcal{W}_{k|k-1}^j, \left\{ (r_{k|k-1}^{j,i}, f_+^{j,i}(\mathbf{y}_k)) \right\}_{i \in \mathbb{I}_+^j} \right) \right\}_{j \in \mathbb{J}_+} \tag{16}$$

where

$$D_+^u(\mathbf{y}_k) = D^b(\mathbf{y}_k) + \langle D^u(\mathbf{y}_k); p_S(\mathbf{y}_k) f(\mathbf{y}_k|\mathbf{y}_{k-1}) \rangle \tag{17}$$

$$r_{k|k-1}^{j,i} = \left\langle f^{j,i}(\mathbf{y}_k); p_S(\mathbf{y}_k) \right\rangle r_{k-1}^{j,i} \tag{18}$$

$$f_+^{j,i}(\mathbf{y}_k) = \frac{\langle f^{j,i}(\mathbf{y}_k); p_S(\mathbf{y}_k) f(\mathbf{y}_k|\mathbf{y}_{k-1}) \rangle}{\left\langle f^{j,i}(\mathbf{y}_k); p_S(\mathbf{y}_k) \right\rangle} \tag{19}$$

$$\mathcal{W}_{k|k-1}^j = \mathcal{W}_{k-1}^j \tag{20}$$

where p_S is the probability of survival, the birth EO at time k is assumed to be a PPP, and the intensity is $D^b(\mathbf{y}_k)$, $f(\mathbf{y}_k|\mathbf{y}_{k-1})$ is a transition probability density, which is described in detail in Section 3.1.

4.3.2. Updated Density of JDTC-PMBM Filter

It is assumed that pseudo measurements and real measurements are independent of each other, given a predicted JDTC-PMBM density with parameters

$$D_+^u(\mathbf{y}_k), \left\{ \left(\mathcal{W}_{k|k-1}^j, \left\{ (r_{k|k-1}^{j,i}, f_+^{j,i}(\mathbf{y}_k)) \right\}_{i \in \mathbb{I}_+^j} \right) \right\}_{j \in \mathbb{J}_+} \tag{21}$$

with the real-measurement set $\mathbf{Z}^{r,k}$, pseudo measurements $\mathbf{Z}_k^{p,c}$ at time k, and the measurement model discussed in Sections 2 and 3.1, the updated JDTC-PMBM density is given by

$$f(\mathbf{Y}_k \mid \mathbf{Z}^{r,k}, \mathbf{Z}_k^{p,c}) = \sum_{\mathbf{Y}_k^u \uplus \mathbf{Y}_k^d = \mathbf{Y}_k} f^u(\mathbf{Y}_k^u) \sum_{j \in \mathbb{J}_+} \sum_{A \in \mathcal{A}^j} \mathcal{W}_{A,k}^j f_A^j\left(\mathbf{Y}_k^d\right) \tag{22}$$

$$f^u(\mathbf{Y}_k^u) = e^{-\langle D^u; 1 \rangle} \prod_{\mathbf{y}_k \in \mathbf{Y}_k^u} D^u(\mathbf{y}_k) \tag{23}$$

$$f_A^j\left(\mathbf{Y}_k^d\right) = \sum_{\uplus_{C \in A} \mathbf{Y}_k^C = \mathbf{Y}_k^d} \prod_{C \in A} f_C^j\left(\mathbf{Y}_k^C\right) \tag{24}$$

where the updated PPP intensity is given by

$$D^u(\mathbf{y}_k) = q_D(\mathbf{y}_k) D_+^u(\mathbf{y}_k) \tag{25}$$

The weight $\mathcal{W}_{A,k}^j$ is given by

$$\mathcal{W}_{A,k}^j = \frac{\mathcal{W}_{k|k-1}^j \prod_{C \in A} \mathcal{L}_{C,k}}{\sum_{j' \in \mathbb{J}} \sum_{A' \in \mathcal{A}^{j'}} \mathcal{W}_{k|k-1}^{j'} \prod_{C' \in A'} \mathcal{L}_{C',k}} \tag{26}$$

$$\mathcal{L}_{C,k} = \begin{cases} \kappa^{\mathbf{C}_c} + \left\langle D_+^u(\mathbf{y}_k); \psi_{\mathbf{C}_c}(\mathbf{y}_k) \psi_{\mathbf{Z}_k^{p,c}}(\mathbf{y}_k) \right\rangle & \text{if } C \cap \mathbb{I}^j = \emptyset, |\mathbf{C}_c| = 1 \\ \left\langle D_+^u(\mathbf{y}_k); \psi_{\mathbf{C}_c}(\mathbf{y}_k) \psi_{\mathbf{Z}_k^{p,c}}(\mathbf{y}_k) \right\rangle & \text{if } C \cap \mathbb{I}^j = \emptyset, |\mathbf{C}_c| > 1 \\ 1 - r_{k|k-1}^{j,i_C} + r_{k|k-1}^{j,i_C} \left\langle f_+^{j,i_c}(\mathbf{y}_k); q_D(\mathbf{y}_k) \right\rangle & \text{if } C \cap \mathbb{I}^j \neq \emptyset, \mathbf{C}_c = \emptyset \\ r_{k|k-1}^{j,i_C} \left\langle f_+^{j,i_C}(\mathbf{y}_k); \psi_{\mathbf{C}_c}(\mathbf{y}_k) \psi_{\mathbf{Z}_k^{p,c}}(\mathbf{y}_k) \right\rangle & \text{if } C \cap \mathbb{I}^j \neq \emptyset, \mathbf{C}_c \neq \emptyset \end{cases} \tag{27}$$

where $\mathbf{C}_c$ is the measurement subset of the real measurements set $\mathbf{Z}^{r,k}$, $\psi_{\mathbf{C}_c}(\mathbf{y}_k)$ is the real measurements likelihood function, and the densities $f_C^j(\mathbf{Y}_k^C)$ are the Bernoulli densities with parameters

$$r_{C,k}^j = \begin{cases} \dfrac{\left\langle D_+^u(\mathbf{y}_k); \psi_{\mathbf{C}_c}(\mathbf{y}_k)\psi_{\mathbf{Z}_k^{p,c}}(\mathbf{y}_k)\right\rangle}{\kappa^{\mathbf{C}_c} + \left\langle D_+^u(\mathbf{y}_k); \psi_{\mathbf{C}_c}(\mathbf{y}_k)\psi_{\mathbf{Z}_k^{p,c}}(\mathbf{y}_k)\right\rangle} & \text{if } C \cap \mathbb{I}^j = \emptyset, |\mathbf{C}_c| = 1 \\ 1 & \text{if } C \cap \mathbb{I}^j = \emptyset, |\mathbf{C}_c| > 1 \\ \dfrac{r_{k|k-1}^{j,i_C}\left\langle f_+^{j,i_C}(\mathbf{y}_k); q_{\mathrm{D}}(\mathbf{y}_k)\right\rangle}{1 - r_{k|k-1}^{j,i_C} + r_{k|k-1}^{j,i_C}\left\langle f_+^{j,i_C}(\mathbf{y}_k); q_{\mathrm{D}}(\mathbf{y}_k)\right\rangle} & \text{if } C \cap \mathbb{I}^j \neq \emptyset, \mathbf{C}_c = \emptyset \\ 1 & \text{if } C \cap \mathbb{I}^j \neq \emptyset, \mathbf{C}_c \neq \emptyset \end{cases} \tag{28}$$

$$f_C^j(\mathbf{y}_k) = \begin{cases} \dfrac{\psi_{\mathbf{C}_c}(\mathbf{y}_k)\psi_{\mathbf{Z}_k^{p,c}}(\mathbf{y}_k)D_+^u(\mathbf{y}_k)}{\left\langle D_+^u(\mathbf{y}_k); \psi_{\mathbf{C}_c}(\mathbf{y}_k)\psi_{\mathbf{Z}_k^{p,c}}(\mathbf{y}_k)\right\rangle} & \text{if } C \cap \mathbb{I}^j = \emptyset, \mathbf{C}_c \neq \emptyset \\ \dfrac{q_{\mathrm{D}}(\mathbf{y}_k)f_+^{j,i_C}(\mathbf{y}_k)}{\left\langle f_+^{j,i_C}(\mathbf{y}_k)q_{\mathrm{D}}(\mathbf{y}_k)\right\rangle} & \text{if } C \cap \mathbb{I}^j \neq \emptyset, \mathbf{C}_c = \emptyset \\ \dfrac{\psi_{\mathbf{C}_c}(\mathbf{y}_k)\psi_{\mathbf{Z}_k^{p,c}}(\mathbf{y}_k)f_+^{j,i_C}(\mathbf{y}_k)}{\left\langle f_+^{j,i_C}(\mathbf{y}_k); \psi_{\mathbf{C}_c}(\mathbf{y}_k)\psi_{\mathbf{Z}_k^{p,c}}(\mathbf{y}_k)\right\rangle} & \text{if } C \cap \mathbb{I}^j \neq \emptyset, \mathbf{C}_c \neq \emptyset \end{cases} \tag{29}$$

4.4. Class Probability Mass Function

We define the measurement set of an EO with state $\mathbf{y}_k$ as $\mathbf{Z}_k = \{\mathbf{C}_c, \mathbf{Z}_k^{p,c}\}$ at time k, and $\mathbf{Z}^k = \{\mathbf{Z}_1, \ldots, \mathbf{Z}_k\}$, then, the class probability mass function (PMF) $p(\mathcal{C}_k^c \big| \mathbf{Z}^k)$ can be obtained, for a PPP with intensity $D^u(\mathbf{y}_k)$, and the class probability mass function is given by

$$\mu_{D^u,k}^{c,\mathbf{C}_c} = \frac{p(\mathcal{C}_k^c|\mathbf{Z}^{k-1}) \int \psi_{\mathbf{C}_c}(\mathbf{y}_k)\psi_{\mathbf{Z}_k^{p,c}}(\mathbf{y}_k)D_+^u(\xi_k|\mathcal{C}_k^c, \mathbf{Z}^{k-1})d\xi_k}{\sum_{c=1}^{n_c} p(\mathcal{C}_k^c|\mathbf{Z}^{k-1}) \int \psi_{\mathbf{C}_c}(\mathbf{y}_k)\psi_{\mathbf{Z}_k^{p,c}}(\mathbf{y}_k)D_+^u(\xi_k|\mathcal{C}_k^c, \mathbf{Z}^{k-1})d\xi_k} \tag{30}$$

for MBM density, the class probability mass function of a detected EO is given by

$$\mu_{j,i_C,k}^{c,\mathbf{C}_c} = \frac{p(\mathcal{C}_k^c|\mathbf{Z}^{k-1}) \int \psi_{\mathbf{C}_c}(\mathbf{y}_k)\psi_{\mathbf{Z}_k^{p,c}}(\mathbf{y}_k)f_+^{j,i_C}(\xi_k|\mathcal{C}_k^c, \mathbf{Z}^{k-1})d\xi_k}{\sum_{c=1}^{n_c} p(\mathcal{C}_k^c|\mathbf{Z}^{k-1}) \int \psi_{\mathbf{C}_c}(\mathbf{y}_k)\psi_{\mathbf{Z}_k^{p,c}}(\mathbf{y}_k)f_+^{j,i_C}(\xi_k|\mathcal{C}_k^c, \mathbf{Z}^{k-1})d\xi_k} \tag{31}$$

The derivation of the class PMF is described in Appendix A.

In order to improve readability, the processing steps of JDTC-PMBM filter are described in Figure 1.

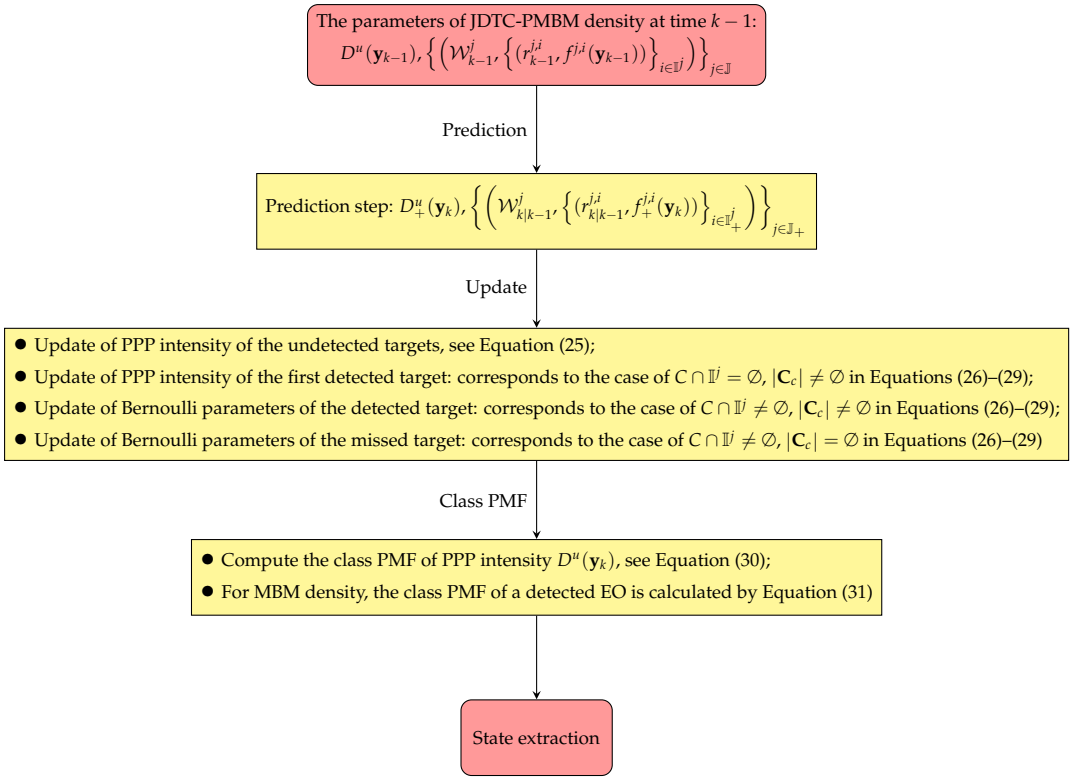

Figure 1. The schematic figure summarising the processing steps of JDTC-PMBM filter.

5. The Implementation Process of the Proposed JDTC-PMBM Filter

In order to analytically implement the JDTC-PMBM filter proposed in Section 4, the kinematics state, extended state, and measurement rate of each EO are described as Gaussian distribution, inverse Wishart distribution, and gamma distribution, respectively [18,26]. The analytical implementation for JDTC-PMBM filter is referred to as JDTC-PMBM-GGIW filter, where all single EO densities in the JDTC-PMBM filter are modeled as the form of the product of GGIW distribution and class PMF.

5.1. Prediction of JDTC-PMBM-GGIW

We assume that the PPP intensity for undetected EOs at time $k-1$ is described as

$$D^u(\mathbf{y}_{k-1}) = \mu^c_{D^u,k-1}\sum_{j=1}^{J_{u,k-1}} w^{c,j}_{u,k-1}\mathcal{GAM}(\gamma_{k-1};\alpha^{c,j}_{u,k-1},\beta^{c,j}_{u,k-1}) \times \mathcal{N}(\mathbf{x}_{k-1};\mathbf{m}^{c,j}_{u,k-1},\mathbf{P}^{c,j}_{u,k-1})\mathcal{IW}(\mathbf{X}_{k-1};v^{c,j}_{u,k-1},\mathbf{V}^{c,j}_{u,k-1}) \tag{32}$$

The birth PPP intensity with known parameters at time $k-1$ is described as

$$D^b(\mathbf{y}_{k-1}) = \mu^c_{D^b,k-1}\sum_{j=1}^{J_{b,k-1}} w^{c,j}_{b,k-1}\mathcal{GAM}(\gamma_{k-1};\alpha^{c,j}_{b,k-1},\beta^{c,j}_{b,k-1}) \times \mathcal{N}(\mathbf{x}_{k-1};\mathbf{m}^{c,j}_{b,k-1},\mathbf{P}^{c,j}_{b,k-1})\mathcal{IW}(\mathbf{X}_{k-1};v^{c,j}_{b,k-1},\mathbf{V}^{c,j}_{b,k-1}) \tag{33}$$

where $\mathcal{IW}(\cdot;v,\mathbf{V})$ denotes the inverse Wishart distribution with freedom degree v and parameter matrix $\mathbf{V}$.

For the MBs in MBM, the spatial probability density $f^{j,i}(\mathbf{y}_{k-1})$ at time $k-1$ is described as

$$\begin{aligned} f^{j,i}(\mathbf{y}_{k-1}) = \mu^c_{j,i,k-1}\mathcal{GAM}(\gamma_{k-1};\alpha^c_{j,i,k-1},\beta^c_{j,i,k-1}) \\ \times \mathcal{N}(\mathbf{x}_{k-1};\mathbf{m}^c_{j,i,k-1},\mathbf{P}^c_{j,i,k-1})\mathcal{IW}(\mathbf{X}_{k-1};v^c_{j,i,k-1},\mathbf{V}^c_{j,i,k-1}) \end{aligned} \tag{34}$$

We define

$$\mathcal{GAM}(\gamma_k;\alpha_k,\beta_k)\mathcal{N}(\mathbf{x}_k;\mathbf{m}_k,\mathbf{P}_k)\mathcal{IW}(\mathbf{X}_k;v_k,\mathbf{V}_k) = \mathcal{GGIW}(\xi_k;\zeta_k) \tag{35}$$

where $\zeta_k = \{\alpha_k,\beta_k,\mathbf{m}_k,\mathbf{P}_k,v_k,\mathbf{V}_k\}$.

As described in Section 4.3.1, the parameters

$$D^u_+(\mathbf{y}_k), \left\{\left(\mathcal{W}^j_{k|k-1}, \left\{(r^{j,i}_{k|k-1}, f^{j,i}_+(\mathbf{y}_k))\right\}_{i\in\mathbb{I}^j_+}\right)\right\}_{j\in\mathbb{J}_+} \tag{36}$$

of the predicted JDTC-PMBM density can be described as

$$D^u_+(\mathbf{y}_k) = D^b(\mathbf{y}_k) + \mu^c_{D^u,k|k-1}\sum_{n=1}^{J_{u,k-1}} w^{c,n}_{u,k|k-1}\mathcal{GGIW}(\xi_k;\zeta^{c,n}_{u,k|k-1}) \tag{37}$$

$$w^{c,n}_{u,k|k-1} = w^{c,n}_{u,k-1}p_S(\mathbf{y}_k) \tag{38}$$

$$\mu^c_{D^u,k|k-1} = \mu^c_{D^u,k-1} \tag{39}$$

$$r^{j,i}_{k|k-1} = p_S(\mathbf{y}_k)r^{j,i}_{k-1} \tag{40}$$

$$f^{j,i}_+(\mathbf{y}_k) = \mu^c_{j,i,k|k-1}\mathcal{GGIW}(\xi_k;\zeta^c_{j,i,k|k-1}) \tag{41}$$

$$\mu^c_{j,i,k|k-1} = \mu^c_{j,i,k-1} \tag{42}$$

$$\mathcal{W}^j_{k|k-1} = \mathcal{W}^j_{k-1} \tag{43}$$

The $\zeta^{c,n}_{u,k|k-1}$ in (37) and $\zeta^c_{j,i,k|k-1}$ in (41) have similar computational processes. The relevant parameters are calculated as follows.

$$\alpha^c_{k|k-1} = \frac{\alpha^c_{k-1}}{\tau}, \quad \beta^c_{k|k-1} = \frac{\beta^c_{k-1}}{\tau} \tag{44}$$

$$\mathbf{m}^c_{k|k-1} = (\mathbf{F}_k)\mathbf{m}^c_{k-1} \tag{45}$$

$$\mathbf{P}^c_{k|k-1} = \mathbf{F}_k\mathbf{P}^c_{k-1}(\mathbf{F}_k)^\top + \mathbf{Q}_k \tag{46}$$

$$v^c_{k|k-1} = \frac{2\delta^c_k(\lambda^c_{k-1}-1)(\lambda^c_{k-1}-2)}{(\lambda^c_{k-1})^2(\lambda^c_{k-1}+1)^{-1}(\lambda^c_{k-1}+\delta^c_k)} + 2d + 4 \tag{47}$$

$$\mathbf{V}^c_{k|k-1} = \frac{\delta^c_k(v^c_{k|k-1}-2d-2)\mathbf{M}_k\mathbf{V}^c_{k-1}(\mathbf{M}_k)^\top}{\lambda^c_{k-1}} \tag{48}$$

$$\lambda^c_{k-1} = v^c_{k-1} - 2d - 2 \tag{49}$$

where δ^c_k is the degree of freedom. The predicted gamma distribution is described by forgetting factor $\frac{1}{\tau}$ in (44) [18], and $\frac{1}{\tau} > 1$. The derivation process of Gaussian inverse Wishart parameters of predicted JDTC-PMBM density is similar to Appendix C of Reference [35].

5.2. Update of JDTC-PMBM-GGIW

As described in Section 4.3.2, the updated JDTC-GGIW-PMBM can be divided into four parts.

(1) **Update of PPP: the undetected targets**

The $D_+^u(\mathbf{y}_k)$ is obtained in the prediction step. The probability of missed detection is $q_{\mathrm{D}}(\mathbf{y}_k)$, and the updated PPP intensity $D^u(\mathbf{y}_k)$ for the undetected targets is given by

$$D_+^u(\mathbf{y}_k) = \mu_{D^u,k|k-1}^c \sum_{n=1}^{J_{u,k|k-1}} (w_{u_1,k|k-1}^{c,n} \mathcal{GGIW}(\xi_k; \zeta_{u_1,k|k-1}^{c,n}) + w_{u_2,k|k-1}^{c,n} \mathcal{GGIW}(\xi_k; \zeta_{u_2,k|k-1}^{c,n})) \tag{50}$$

where

$$J_{u,k|k-1} = J_{b,k-1} + J_{u,k-1} \tag{51}$$

$$w_{u_1,k|k-1}^{c,n} = (1 - p_{\mathrm{D}}(\mathbf{y}_k)) w_{u,k|k-1}^{c,n} \tag{52}$$

$$w_{u_2,k|k-1}^{c,n} = p_{\mathrm{D}}(\mathbf{y}_k) \left(\frac{\beta_{u,k|k-1}^{c,n}}{\beta_{u,k|k-1}^{c,n} + 1} \right)^{\alpha_{u,k|k-1}^{c,n}} w_{u,k|k-1}^{c,n} \tag{53}$$

$$\zeta_{u_1,k|k-1}^{c,n} = \zeta_{u,k|k-1}^{c,n} \tag{54}$$

$$\zeta_{u_2,k|k-1}^{c,n} = \{\alpha_{u,k|k-1}^{c,n}, \beta_{u,k|k-1}^{c,n} + 1, \mathbf{m}_{u,k|k-1}^{c,n}, \mathbf{P}_{u,k|k-1}^{c,n}, v_{u,k|k-1}^{c,n}, \mathbf{V}_{u,k|k-1}^{c,n}\} \tag{55}$$

As described in Reference [18], the bi-modality of the γ_k estimate in (50) can be reduced to a single mode by using gamma mixture reduction.

(2) **Update of PPP: the first detected target**

The target is detected for the first time, and a detection measurement set $\mathbf{C}_c$ is generated. This case corresponds to the case $C \cap \mathbb{I}^j = \emptyset, \mathbf{C}_c \neq \emptyset$ in Section 4.3.2. Given the predicted PPP intensity $D_+^u(\mathbf{y}_k)$ in (37), the existence probability and spatial distribution are given by

$$r_{\mathbf{C}_c,k}^u = \begin{cases} 1 & \text{if} \quad |\mathbf{C}_c| > 1 \\ \frac{\mathcal{L}_{\mathbf{C}_c,k}^u}{\kappa^{\mathbf{C}_c} + \mathcal{L}_{\mathbf{C}_c,k}^u} & \text{if} \quad |\mathbf{C}_c| = 1 \end{cases} \tag{56}$$

$$f_{\mathbf{C}_c}^u(\mathbf{y}_k) = \frac{\psi_{\mathbf{C}_c}(\mathbf{y}_k) \psi_{\mathbf{Z}_k^{p,c}}(\mathbf{y}_k) D_+^u(\mathbf{y}_k)}{\left\langle D_+^u(\mathbf{y}_k); \psi_{\mathbf{C}_c}(\mathbf{y}_k) \psi_{\mathbf{Z}_k^{p,c}}(\mathbf{y}_k) \right\rangle} \tag{57}$$

$$= \mu_{D^u,k}^{c,\mathbf{C}_c} \sum_{n=1}^{J_{u,k|k-1}} w_{u,k}^{c,\mathbf{C}_c,n} \mathcal{GGIW}(\mathbf{y}_k; \zeta_{u,k}^{c,\mathbf{C}_c,n}) \tag{58}$$

where

$$\mu_{D^u,k}^{c,\mathbf{C}_c} = \frac{\mu_{D^u,k|k-1}^c \sum_{n=1}^{J_{u,k|k-1}} w_{u,k|k-1}^{c,n} Q_k^{c,\mathbf{C}_c,n} G_k^{c,\mathbf{C}_c,n} \Delta_k^{c,\mathbf{C}_c,n}}{\sum_{c=1}^{n_c} \mu_{D^u,k|k-1}^c \sum_{n=1}^{J_{u,k|k-1}} w_{u,k|k-1}^{c,n} Q_k^{c,\mathbf{C}_c,n} G_k^{c,\mathbf{C}_c,n} \Delta_k^{c,\mathbf{C}_c,n}} \tag{59}$$

$$w_{u,k}^{c,\mathbf{C}_c,n} = \frac{w_{u,k|k-1}^{c,n} Q_k^{c,\mathbf{C}_c,n} G_k^{c,\mathbf{C}_c,n} \Delta_k^{c,\mathbf{C}_c,n}}{\sum_{n=1}^{J_{u,k|k-1}} w_{u,k|k-1}^{c,n} Q_k^{c,\mathbf{C}_c,n} G_k^{c,\mathbf{C}_c,n} \Delta_k^{c,\mathbf{C}_c,n}} \tag{60}$$

$$\mathcal{L}_{\mathbf{C}_c,k}^u = \sum_{c=1}^{n_c} \mu_{D^u,k|k-1}^c \sum_{n=1}^{J_{u,k|k-1}} w_{u,k|k-1}^{c,n} Q_k^{c,\mathbf{C}_c,n} G_k^{c,\mathbf{C}_c,n} \Delta_k^{c,\mathbf{C}_c,n} \tag{61}$$

where $\zeta_{u,k}^{c,\mathbf{C}_c,n} = \{\alpha_{u,k}^{c,\mathbf{C}_c,n}, \beta_{u,k}^{c,\mathbf{C}_c,n}, \mathbf{m}_{u,k}^{c,\mathbf{C}_c,n}, \mathbf{P}_{u,k}^{c,\mathbf{C}_c,n}, v_{u,k}^{c,\mathbf{C}_c,n}, \mathbf{V}_{u,k}^{c,\mathbf{C}_c,n}\}$, $Q_k^{c,\mathbf{C}_c,n}$, $G_k^{c,\mathbf{C}_c,n}$, $\Delta_k^{c,\mathbf{C}_c,n}$ are computed as in Table 1, and $J_{u,k|k-1}$ is the number of GGIW components of $D_+^u(\mathbf{y}_k)$. The proof of the derivation of the parameters can be found in Appendix B.

(3) **Update of Bernoulli: the detected target**

The case $C \cap \mathbb{I}^j \neq \emptyset, \mathbf{C}_c \neq \emptyset$ in Section 4.3.2 means that the i_C-th EO of the j-th global hypothesis is detected again at time k, and the measurement set of the detections is $\mathbf{C}_c$. Given the predicted existence probability $r_{k|k-1}^{j,i_C}$, and spatial density $f_+^{j,i_C}(\mathbf{y}_k)$ of the i_C-th Bernoulli of the j-th MB component, the updated existence probability and updated spatial distribution of the i_C-th Bernoulli of the j-th MB component are given by

$$r_{\mathbf{C}_c,k}^{j,i_C} = 1 \tag{62}$$

$$f_{\mathbf{C}_c}^{j,i_C}(\mathbf{y}_k|\mathbf{Z}^k) = \mu_{j,i_C,k}^{c,\mathbf{C}_c} \mathcal{GGIW}(\mathbf{y}_k; \zeta_{j,i_C,k}^{c,\mathbf{C}_c}) \tag{63}$$

where

$$\mu_{j,i_C,k}^{c,\mathbf{C}_c} = \frac{\mu_{j,i_C,k|k-1}^{c} Q_k^{c,\mathbf{C}_c} G_k^{c,\mathbf{C}_c} \Delta_k^{c,\mathbf{C}_c}}{\sum_{c=1}^{n_c} \mu_{j,i_C,k|k-1}^{c} Q_k^{c,\mathbf{C}_c} G_k^{c,\mathbf{C}_c} \Delta_k^{c,\mathbf{C}_c}} \tag{64}$$

$\zeta_{j,i_C,k}^{c,\mathbf{C}_c} = \{\alpha_{j,i_C,k}^{c,\mathbf{C}_c}, \beta_{j,i_C,k}^{c,\mathbf{C}_c}, \mathbf{m}_{j,i_C,k}^{c,\mathbf{C}_c}, \mathbf{P}_{j,i_C,k}^{c,\mathbf{C}_c}, v_{j,i_C,k}^{c,\mathbf{C}_c}, \mathbf{V}_{j,i_C,k}^{c,\mathbf{C}_c}\}$, $Q_k^{c,\mathbf{C}_c}$, $G_k^{c,\mathbf{C}_c}$, $\Delta_k^{c,\mathbf{C}_c}$ are computed as in Table 1. The likelihood $\mathcal{L}_{\mathbf{C}_c,k}^{j,i_C}$ is given by

$$\begin{aligned} \mathcal{L}_{\mathbf{C}_c,k}^{j,i_C} &= r_{k|k-1}^{j,i_C} \left\langle f_+^{j,i_C}(\mathbf{y}_k); \psi_{\mathbf{C}_c}(\mathbf{y}_k) \psi_{\mathbf{Z}_k^{p,c}}(\mathbf{y}_k) \right\rangle \\ &= r_{k|k-1}^{j,i_C} \sum_{c=1}^{n_c} \mu_{j,i_C,k|k-1}^{c} Q_k^{c,\mathbf{C}_c} G_k^{c,\mathbf{C}_c} \Delta_k^{c,\mathbf{C}_c} \end{aligned} \tag{65}$$

The proof of the parameters derivation can be found in Appendix B.

(4) **Update of Bernoulli: the missed target**

The case for an EO that was previously detected but is missed at time k corresponds to $C \cap \mathbb{I}^j \neq \emptyset, \mathbf{C}_c = \emptyset$ in Section 4.3.2. Given the predicted existence probability $r_{k|k-1}^{j,i}$, spatial density $f_+^{j,i}(\mathbf{y}_k)$ of the i-th Bernoulli of the j-th MB component, and the empty measurements set, the updated existence probability is given by

$$r_{\emptyset,k}^{j,i} = \frac{r_{k|k-1}^{j,i} \sum_{c=1}^{n_c} \mu_{j,i,k|k-1}^{c} q_{D,k}^{j,i,c}}{1 - r_{k|k-1}^{j,i} + r_{k|k-1}^{j,i} \sum_{c=1}^{n_c} \mu_{j,i,k|k-1}^{c} q_{D,k}^{j,i,c}} \tag{66}$$

where

$$q_{D,k}^{j,i,c} = 1 - p_D(\mathbf{y}_k) + p_D(\mathbf{y}_k) \left(\frac{\beta_{j,i,k|k-1}^{c}}{\beta_{j,i,k|k-1}^{c} + 1} \right)^{\alpha_{j,i,k|k-1}^{c}} \tag{67}$$

the existence probability is given by probability that the EO exists but is not detected, $r_{k|k-1}^{j,i} q_{D,k}^{j,i}$, or the EO is not existing, $1 - r_{k|k-1}^{j,i}$.

The updating spatial density is given by

$$f_{\emptyset}^{j,i}(\mathbf{y}_k) = \mu_{j,i,k}^{c} (w_{a,j,i,k}^{c} \mathcal{GGIW}(\mathbf{y}_k; \zeta_{a,j,i,k}^{c}) + w_{b,j,i,k}^{c} \mathcal{GGIW}(\mathbf{y}_k; \zeta_{b,j,i,k}^{c})) \tag{68}$$

where

$$\begin{aligned}
\mu^c_{j,i,k} &= \mu^c_{j,i,k|k-1} \\
w^c_{a,j,i,k} &= (\sum_{c=1}^{n_c} \mu^c_{j,i,k|k-1} q^{j,i,c}_{D,k})^{-1}(1 - p_D(\mathbf{y}_k)) \\
w^c_{b,j,i,k} &= (\sum_{c=1}^{n_c} \mu^c_{j,i,k|k-1} q^{j,i,c}_{D,k})^{-1} p_D(\mathbf{y}_k) \left(\frac{\beta^c_{j,i,k|k-1}}{\beta^c_{j,i,k|k-1}+1} \right)^{\alpha^c_{j,i,k|k-1}} \\
\zeta^c_{a,j,i,k} &= \zeta^c_{j,i,k|k-1} \\
\zeta^c_{b,j,i,k} &= \{\alpha^c_{j,i,k|k-1}, \beta^c_{j,i,k|k-1}+1, \mathbf{m}^c_{j,i,k|k-1}, \mathbf{P}^c_{j,i,k|k-1}, v^c_{j,i,k|k-1}, \mathbf{V}^c_{j,i,k|k-1}\}
\end{aligned} \tag{69}$$

For the detected EO, there are two possible situations that cause the measurement set to be empty: the EO generates an empty measurement set and the EO is missed. Thus, the updated spatial density is bi-modal. The gamma mixture reduction method of reducing bi-modal distribution to an unimodal is described in detail in Reference [18]. The likelihood $\mathcal{L}^{j,i}_{\emptyset,k}$ is given by

$$\mathcal{L}^{j,i}_{\emptyset,k} = 1 - r^{j,i}_{k|k-1} + r^{j,i}_{k|k-1} \sum_{c=1}^{n_c} \mu^c_{j,i,k|k-1} q^{j,i,c}_{D,k} \tag{70}$$

Table 1. The GGIW parameters in the implementation process.

$$\begin{aligned}
&\alpha^{c,\mathbf{C}_c}_k = \alpha^c_{k|k-1} + |\mathbf{C}_c|, \qquad \beta^{c,\mathbf{C}_c}_k = \beta^c_{k|k-1} + 1 \\
&\mathbf{S}^{c,\mathbf{C}_c}_{k|k-1} = \mathbf{H}_k \mathbf{P}^c_{k|k-1} (\mathbf{H}_k)^\top + \frac{\mathbf{B}_k \overline{\mathbf{X}}_{k|k-1} (\mathbf{B}_k)^\top}{|\mathbf{C}_c|} \\
&K^{(c,\mathbf{C}_c)}_{k|k-1} = \mathbf{P}^c_{k|k-1} (\mathbf{H}_k)^\top (\mathbf{S}^{c,\mathbf{C}_c}_{k|k-1})^{-1} \\
&\varepsilon^{(c,\mathbf{C}_c)}_{k|k-1} = \bar{\mathbf{z}}^{\mathbf{C}_c}_k - (\mathbf{H}_k)\mathbf{m}^c_{k|k-1} \\
&\mathbf{m}^{c,\mathbf{C}_c}_k = \mathbf{m}^c_{k|k-1} + (K^{(c,\mathbf{C}_c)}_{k|k-1}) \varepsilon^{(c,\mathbf{C}_c)}_{k|k-1} \\
&\mathbf{P}^{c,\mathbf{C}_c}_k = \mathbf{P}^c_{k|k-1} - K^{(c,\mathbf{C}_c)}_{k|k-1} \mathbf{H}_k \mathbf{P}^c_{k|k-1} \\
&\varepsilon^{(c,\mathbf{C}_c)}_{k|k-1} = \bar{\mathbf{z}}^{\mathbf{C}_c}_k - (\mathbf{H}_k)\mathbf{m}^c_{k|k-1} \\
&v^{c,\mathbf{C}_c}_k = v^c_{k|k-1} + |\mathbf{C}_c| + \delta^{p,c}_k \\
&\mathbf{V}^{c,\mathbf{C}_c}_k = \mathbf{V}^c_{k|k-1} + \mathbf{N}^{c,\mathbf{C}_c}_k + (\mathbf{B}_k)^{-1} \mathbf{Z}^{\mathbf{C}_c}_k (\mathbf{B}_k)^{-\top} \\
&+\delta^{p,c}_k (\mathbf{E}^c_k)^{-1} \mathbf{Z}^{p,c}_k (\mathbf{E}^c_k)^{-\top} \\
&\mathbf{N}^{c,\mathbf{C}_c}_k = \varepsilon^{(c,\mathbf{C}_c)}_{k|k-1} (\varepsilon^{(c,\mathbf{C}_c)}_{k|k-1})^\top (\mathbf{S}^{c,\mathbf{C}_c}_{k|k-1,j})^{-1} \overline{\mathbf{X}}_{k|k-1} \\
&\mathbf{B}_k = (\mathbf{R}_k + \eta \overline{\mathbf{X}}_{k|k-1})^{1/2} (\overline{\mathbf{X}}_{k|k-1})^{-1/2} \\
&\bar{\mathbf{z}}^{\mathbf{C}_c}_k = \frac{1}{|\mathbf{C}_c|} \sum_{j=1}^{|\mathbf{C}_c|} \mathbf{z}^{\mathbf{C}_c}_j \\
&\mathbf{Z}^{\mathbf{C}_c}_k = \sum_{j=1}^{|\mathbf{C}_c|} (\mathbf{z}^{\mathbf{C}_c}_j - \bar{\mathbf{z}}^{\mathbf{C}_c}_k)(\mathbf{z}^{\mathbf{C}_c}_j - \bar{\mathbf{z}}^{\mathbf{C}_c}_k)^\top \\
&G^{c,\mathbf{C}_c}_k = \frac{\Gamma(\alpha^c_{k|k-1}+|\mathbf{C}_c|)(\beta^c_{k|k-1})^{\alpha^c_{k|k-1}}}{\Gamma(\alpha^c_{k|k-1})(\beta^c_{k|k-1}+1)^{\alpha^c_{k|k-1}+|\mathbf{C}_c|}|\mathbf{C}_c|!} \\
&Q^{c,\mathbf{C}_c}_k \triangleq p_D(\mathbf{y}_k) e^{-\gamma_{k|k-1}} (\gamma_{k|k-1})^{|\mathbf{C}_c|} \\
&\Delta^{c,\mathbf{C}_c}_k = \frac{2^{\frac{(|\mathbf{C}_c|+\delta^{p,c}_k)(1-d)}{2}} |\mathbf{Z}^{p,c}_k|^{\frac{\delta^{p,c}_k-d-1}{2}} |\delta^{p,c}_k|^{\frac{\delta^{p,c}_k}{2}}}{\pi^{\frac{(|\mathbf{C}_c|d)}{2}} (|\mathbf{C}_c|)^{\frac{d}{2}} |\mathbf{B}_k|^{|\mathbf{C}_c|-1} |\mathbf{S}^{c,\mathbf{C}_c}_{k|k-1} (\overline{\mathbf{X}}_{k|k-1})^{-1}|^{\frac{1}{2}}} \frac{|\mathbf{V}^c_{k|k-1}|^{\frac{v^c_{k|k-1}-d-1}{2}}}{|\mathbf{V}^{c,\mathbf{C}_c}_k|^{\frac{v^c_{k|k-1}+|\mathbf{C}_c|+\delta^{p,c}_k-d-1}{2}}} \\
&\qquad \times \frac{\Gamma_d(\frac{v^c_{k|k-1}+|\mathbf{C}_c|+\delta^{p,c}_k-d-1}{2})}{\Gamma_d(\frac{v^c_{k|k-1}-d-1}{2})\Gamma_d(\frac{\delta^{p,c}_k}{2})}
\end{aligned}$$

6. Results

In order to verify the effectiveness of the proposed JDTC-PMBM-GGIW algorithm, this section first introduces the evaluation metrics and simulation scenarios. Then it gives the simulation performance comparison results between the proposed JDTC-PMBM-GGIW algorithm and the existing RFS-based JDTC methods [35,36]. The construction of simulation scenarios is motivated by References [7,15,35,41]. The flow chart of the proposed JDTC-PMBM-GGIW filter in Section 5 is shown in Figure 2.

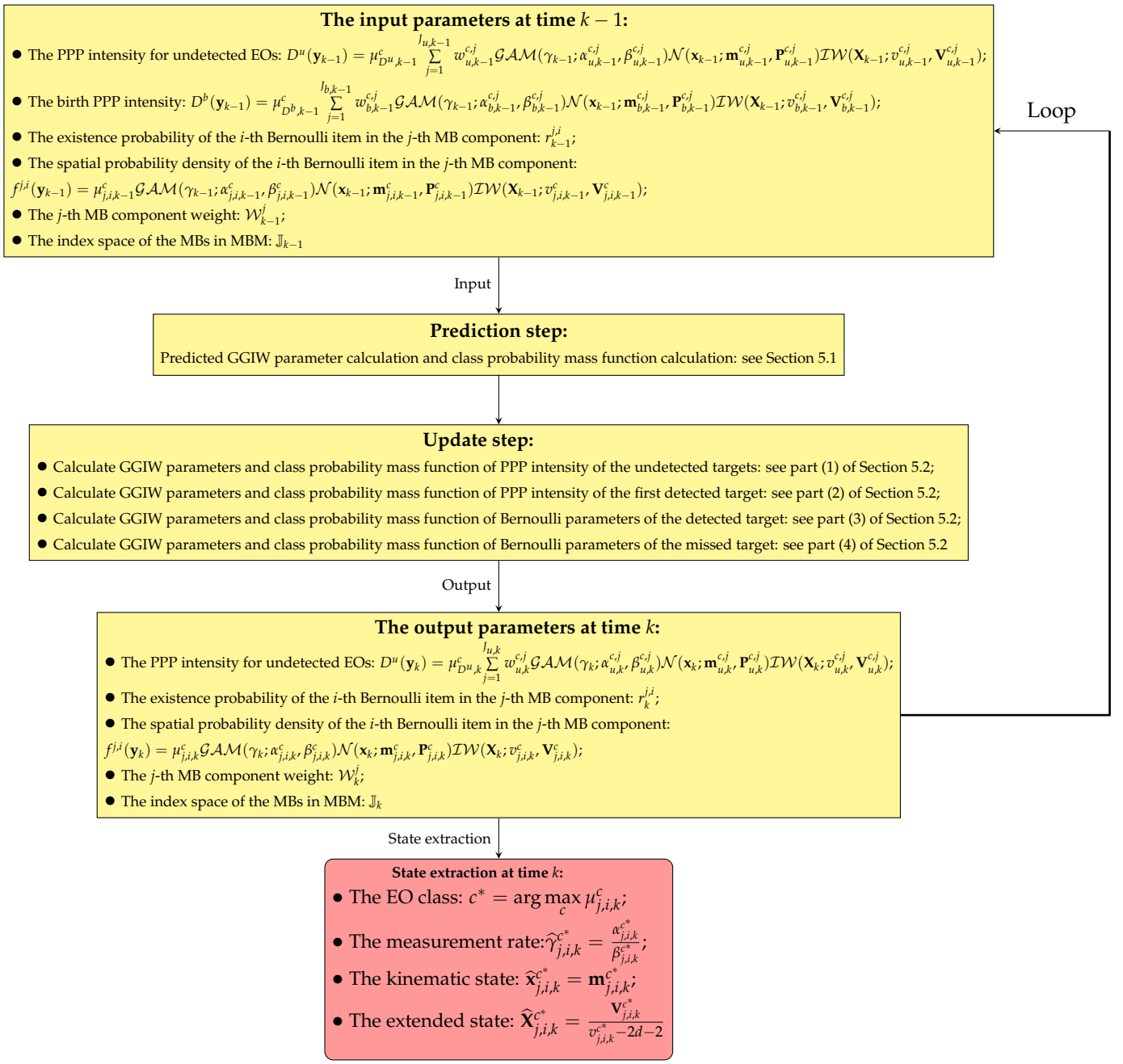

Figure 2. The flow chart of the proposed JDTC-PMBM-GGIW filter in Section 5.

6.1. Performance Evaluation Metrics

In this paper, the optimal sub-pattern assignment (OSPA) distance is adopted to evaluate the tracking performance of the proposed JDTC-PMBM-GGIW filter. The OSPA distance is described as

$$\bar{d}_p^{(c)}(\mathbf{Y},\hat{\mathbf{Y}})=\left(\frac{1}{n_o}\left(\sum_{k=1}^{m_o}\left(d^{(c)}(\mathbf{y}_k,\hat{\mathbf{y}}_{\pi(k)})\right)^p+c^p(n_o-m_o)\right)\right)^{1/p} \tag{71}$$

where

$$\pi(k)=\arg\min_{\pi\in\Pi_{n_o}}\sum_{k=1}^{m_o}\left(d^{(c)}(\mathbf{y}_k,\hat{\mathbf{y}}_j)\right)^p \tag{72}$$

$$d^{(c)}(\mathbf{y}_k,\hat{\mathbf{y}}_j)=\min(c,d(\mathbf{y}_k,\hat{\mathbf{y}}_j)) \tag{73}$$

where $\pi(k)$ is an optimal assignment, $m_o \le n_o, \mathbf{Y}=\{\mathbf{y}_1,\cdots,\mathbf{y}_{m_o}\}$ is the real EO state set, and $\hat{\mathbf{Y}}=\{\hat{\mathbf{y}}_1,\cdots,\hat{\mathbf{y}}_{n_o}\}$ is the estimated EO state set, the order p and cut-off c satisfy $1\le p<\infty$ and $c>0$. If $m_o>n_o$, $\bar{d}_p^{(c)}(\mathbf{Y},\hat{\mathbf{Y}})=\bar{d}_p^{(c)}(\hat{\mathbf{Y}},\mathbf{Y})$. Π_{n_o} denotes the all permutations on $\{1,2,\ldots,n_o\}$.

The true extended objects' parameters set at time k is $\{\xi_k^{(i)}\}_{i=1}^{N_{X,k}}$, where $\xi_k^{(i)}=(\gamma_k^{(i)},\mathbf{x}_k^{(i)},\mathbf{X}_k^{(i)})$ and $N_{X,k}$ is the true number of objects. The estimated extended objects' parameters set is $\{\hat{\xi}_k^{(j)}\}_{j=1}^{M_k'}$, where $\hat{\xi}_k^{(i)}=(\hat{\gamma}_k^{(i)},\hat{\mathbf{x}}_k^{(i)},\hat{\mathbf{X}}_k^{(i)})$. The OSPA distance between the set $\{\xi_k^{(i)}\}_{i=1}^{N_{X,k}}$ and the set $\{\hat{\xi}_k^{(j)}\}_{j=1}^{M_k'}$ is computed by (71), where $m=N_{x,k}$, $n=M_k'$, $d^{(c)}(\mathbf{y}_i,\hat{\mathbf{y}}_{\pi(i)})$ is, respectively, defined as

$$d^{(c_\gamma)}(\gamma_k^{(i)},\hat{\gamma}_k^{(\pi(i))})=\min(c_\gamma,\|\gamma_k^{(i)}-\hat{\gamma}_k^{(\pi(i))}\|_2) \tag{74}$$

$$d^{(c_\mathbf{x})}(\mathbf{x}_k^{(i)},\hat{\mathbf{x}}_k^{(\pi(i))})=\min(c_\mathbf{x},\|\mathbf{x}_k^{(i)}-\hat{\mathbf{x}}_k^{(\pi(i))}\|_2) \tag{75}$$

$$d^{(c\mathbf{x})}(\mathbf{X}_k^{(i)},\hat{\mathbf{X}}_k^{(\pi(i))})=\min(c_\mathbf{X},\|\mathbf{X}_k^{(i)}-\hat{\mathbf{X}}_k^{(\pi(i))}\|_F) \tag{76}$$

where $\|\cdot\|_2$ denotes the Euclidean norm, $\|\cdot\|_F$ denotes the Frobenius norm.

6.2. Simulation Scenario Setting

The monitoring area is 2000 m × 2000 m. The simulation results are obtained from 500 Monte Carlo simulation experiments. The measurement noise covariance $\mathbf{R}_n=\mathrm{diag}([1\ \mathrm{m}^2/\mathrm{s}^2, 1\ \mathrm{m}^2/\mathrm{s}^2])$, and the regulation parameter of the sensor between the covariance $\mathbf{R}_n$ and the extended state $\mathbf{X}_k$ is set to $\lambda_n=1/4$. The detection probability $P_d=0.9$, the birth probability of EOs $p^{\mathrm{b}}=0.01$, and the survival probability of EOs $p_k^{\mathrm{s}}=0.9$, $1/\tau=0.5$, $\delta_k^c=10$.

Similar to References [35,36,46], we assume that the EOs have two categories, and the size matrix of the first class EOs is described as $\mathbf{Z}_k^{p,1}=\mathrm{diag}(170^2\ \mathrm{m}^2, 40^2\ \mathrm{m}^2)$, the size matrix of the second class EOs is $\mathbf{Z}_k^{p,2}=\mathrm{diag}(70^2\ \mathrm{m}^2, 7.5^2\ \mathrm{m}^2)$. The measurement rates of the first class EOs and the second class EOs are respectively set as 30 and 20. Bernoulli components with an existence probability less than 0.5 is pruned. For the mixture GGIW components of PPP intensity, the pruning and merging thresholds are set to $T_g=10^{-3}$ and $T_u=4$, respectively. Other parameter settings are the same as in References [35,41].

The kinematics state transition model is linear, and the kinematics state transition equation of an EO is given by

$$\mathbf{x}_k=\mathbf{F}_k(\mathbf{x}_{k-1})+\mathbf{v}_k \tag{77}$$

where $\mathbf{v}_k$ is the process noise following Gaussian distribution with zero mean and covariance matrix $\mathbf{Q}$. Thus, the kinematics state transition probability density function is obtained by

$$f_{k|k-1}(\mathbf{x}_k|\mathbf{x}_{k-1}) = \mathcal{N}(\mathbf{x}_k; \mathbf{F}_{k-1}\mathbf{x}_{k-1}, \mathbf{Q}) \tag{78}$$

In principle, the near-constant velocity (NCV) model and near-constant turn (NCT) model can be used to describe any type of movement, as long as the sampling interval is sufficiently small. Thus, the dynamic model can be described in detail as follows.

- NCV Model:

$$\mathbf{F}_k = \begin{bmatrix} 1 & T_s & 0 & 0 \\ 0 & 1 & 0 & 0 \\ 0 & 0 & 1 & T_s \\ 0 & 0 & 0 & 1 \end{bmatrix} \tag{79}$$

$$\mathbf{Q}_{NCV} = q_{\tau_1} \begin{bmatrix} T_s^3/3 & T_s^2/2 & 0 & 0 \\ T_s^2/2 & T_s & 0 & 0 \\ 0 & 0 & T_s^3/3 & T_s^2/2 \\ 0 & 0 & T_s^2/2 & T_s \end{bmatrix} \tag{80}$$

where $q_{\tau_1} = 0.016$.

- NCT Model:

$$\mathbf{F}_k = \begin{bmatrix} 1 & \sin(T_s\omega)/\omega & 0 & -(1-\cos(T_s\omega))/\omega \\ 0 & \cos(T_s\omega) & 0 & -\sin(T_s\omega) \\ 0 & (1-\cos(T_s\omega))/\omega & 1 & \sin(T_s\omega)/\omega \\ 0 & \sin(T_s\omega) & 0 & \cos(T_s\omega) \end{bmatrix} \tag{81}$$

$$\mathbf{Q}_{NCT} = q_{\tau_2} \begin{bmatrix} T_s^4/4 & T_s^3/2 & 0 & 0 \\ T_s^3/2 & T_s^2 & 0 & 0 \\ 0 & 0 & T_s^4/4 & T_s^3/2 \\ 0 & 0 & T_s^3/2 & T_s^2 \end{bmatrix} \tag{82}$$

where $q_{\tau_2} = 0.0016$, ω denotes the rotational angular velocity and T_s denotes the sampling period.

At time $k = 0$, the initial assumptions of the proposed JDTC-PMBM-GGIW filter are shown in Table 2. The parameters for the two simulation scenarios are set as follows.

Table 2. The initial assumptions of the proposed JDTC-PMBM-GGIW filter.

• The initial birth PPP intensity at time $k = 0$ is given by
$D^b(\mathbf{y}_k) = \mu^c_{D^b,k} \sum_{j=1}^{J_{b,k}} w^{c,j}_{b,k} \mathcal{GAM}(\gamma_k; \alpha^{c,j}_{b,k}, \beta^{c,j}_{b,k-1}) \mathcal{N}(\mathbf{x}_k; \mathbf{m}^{c,j}_{b,k}, \mathbf{P}^{c,j}_{b,k}) \mathcal{IW}(\mathbf{X}_k; v^{c,j}_{b,k}, \mathbf{V}^{c,j}_{b,k})$
• The initial PPP intensity for undetected EOs at time $k = 0$ is described as $D^u(\mathbf{y}_k) = D^b(\mathbf{y}_k)$.
• The initial MBM parameters: $\mathbb{I}_0 = \{j_0\}$, $\mathcal{W}_0^{j_0} = 1$, and $\mathbb{I}_0^{j_0} = \emptyset$.
• The spatial distribution of clutter $c(\mathbf{z})$ is uniform, $c(\mathbf{z}) = A^{-1}$, where A is volume of the surveillance area.

- In scenario 1, there are five EOs in the surveillance area, The actual trajectory of each EO is shown in Figure 3a. The trajectory parameters of each EO of scenario 1 are described in Table 3. The mixture GGIW and class parameters of initial birth PPP intensity are given by

$$\mu^{c}_{D^b,k} = 0.5, \quad w^{c,j}_{b,k} = 0.01 \tag{83}$$
$$\mathbf{m}^{c,1}_{b,k} = [300\ \text{m}, 8\ \text{m/s}, 500\ \text{m}, -8\ \text{m/s}]^\top \tag{84}$$
$$\mathbf{m}^{c,2}_{b,k} = [0\ \text{m}, 8\ \text{m/s}, 0\ \text{m}, 8\ \text{m/s}]^\top \tag{85}$$
$$\mathbf{m}^{c,3}_{b,k} = [800\ \text{m}, 8\ \text{m/s}, 800\ \text{m}, -4\ \text{m/s}]^\top \tag{86}$$
$$\mathbf{m}^{c,4}_{b,k} = [-200\ \text{m}, -8\ \text{m/s}, -250\ \text{m}, 6\ \text{m/s}]^\top \tag{87}$$
$$\mathbf{m}^{c,5}_{b,k} = [-250\ \text{m}, 8\ \text{m/s}, -250\ \text{m}, 6\ \text{m/s}]^\top \tag{88}$$
$$\mathbf{P}^{c,j}_{b,k} = \text{diag}([10^2\ \text{m}^2, 10^2\ \text{m}^2/\text{s}^2, 10^2\ \text{m}^2, 10^2\ \text{m}^2/\text{s}^2]) \tag{89}$$
$$\alpha^{c,j}_{b,k} = 20, \quad \beta^{c,j}_{b,k} = 10, \quad v^{c,j}_{b,k} = 10, \tag{90}$$
$$\mathbf{V}^{c,j}_{b,k} = \text{diag}([1\ 1]), \quad n_c = 2, \quad J_{b,k} = 4. \tag{91}$$

where $J_{b,k}$ denotes the number of birth GGIW components.

- In scenario 2, there are three EOs in the surveillance area, The actual trajectory of each EO is shown in Figure 3b. The trajectory parameters of each EO of scenario 2 are described in Table 4. The mixture GGIW and class parameters of initial birth PPP intensity are given by

$$\mu^{c}_{D^b,k} = 0.5, \quad w^{c,j}_{b,k} = 0.01 \tag{92}$$
$$\mathbf{m}^{c,1}_{b,k} = [-1300\ \text{m}, 5\ \text{m/s}, 500\ \text{m}, -5\ \text{m/s}]^\top \tag{93}$$
$$\mathbf{m}^{c,2}_{b,k} = [50\ \text{m}, 8\ \text{m/s}, 50\ \text{m}, 8\ \text{m/s}]^\top \tag{94}$$
$$\mathbf{m}^{c,3}_{b,k} = [-550\ \text{m}, -6\ \text{m/s}, -650\ \text{m}, 6\ \text{m/s}]^\top \tag{95}$$
$$\mathbf{P}^{c,j}_{b,k} = \text{diag}([10^2\ \text{m}^2, 10^2\ \text{m}^2/\text{s}^2, 10^2\ \text{m}^2, 10^2\ \text{m}^2/\text{s}^2]) \tag{96}$$
$$\alpha^{c,j}_{b,k} = 20, \quad \beta^{c,j}_{b,k} = 10, \quad v^{c,j}_{b,k} = 10 \tag{97}$$
$$\mathbf{V}^{c,j}_{b,k} = \text{diag}([1\ 1]), \quad J_{b,k} = 3, \quad n_c = 2. \tag{98}$$

where $J_{b,k}$ denotes the number of birth GGIW components.

Table 3. Trajectory parameters of each EO of scenario 1.

Target	Model	Birth Time	Death Time	Class
1	NCV	1 s	80 s	1
2	NCV	1 s	80 s	2
3	NCV	1 s	80 s	1
4	NCV	10 s	30 s	1
5	NCV	50 s	70 s	2

Table 4. Trajectory parameters of each EO of scenario 2.

Target	Models	Model Duration Time	Birth Time	Death Time	Class
1	NCV NCT	1–15 s, 32–50 s, 67–80 s 16–31 s, 51–66 s	1 s	80 s	1
2	NCV NCT	1–15 s, 32–50 s, 67–80 s 16–31 s, 51–66 s	1 s	80 s	2
3	NCV NCT	1–15 s, 32–50 s, 67–80 s 16–31 s, 51–66 s	1 s	80 s	1

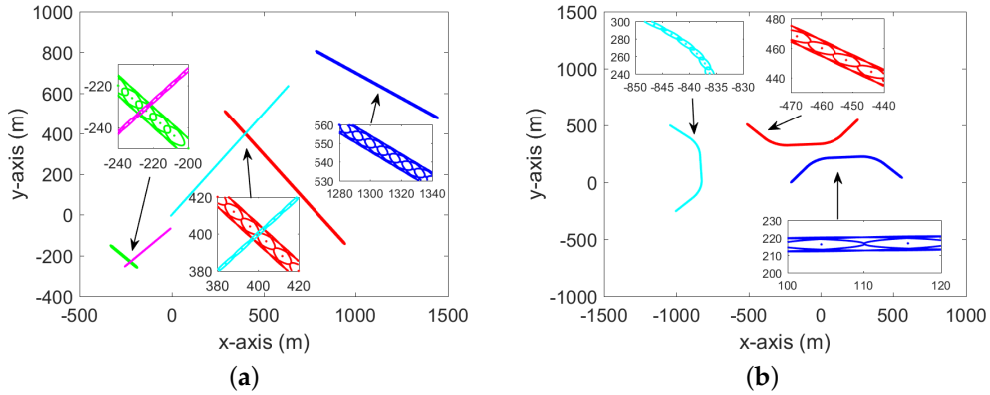

Figure 3. Simulation scenarios. (**a**) The first scenario: target 1, yellow ellipse, class 1; target 2, cyan ellipse, class 2; target 3, blue ellipse, class 1; target 4, green ellipse, class 1; target 5, purple ellipse, class 2. (**b**) The second scenario: target 1, yellow ellipse, class 1; target 2, cyan ellipse, class 2; target 3, blue ellipse, class 1.

6.3. Simulation Results

The programming language used in the simulation experiment is MATLAB. The framework and flow charts of the simulation experiment of the proposed JDTC-PMBM-GGIW algorithm are shown in Figures 1 and 2. The simulation experiments were run on a desktop with CPU i5-44303.00 [GHz] and 16 [GB] RAM memory. The simulation results are as follows.

6.3.1. Scenario 1

The tracking performance of the proposed JDTC-PMBM-GGIW filter, JDTC-GIW-MeMBer filter [35] and JDTC-GIW-PHD filter [36] is shown in Figure 4a–c. In the case that all three methods use prior size information, the OSPA distance of measurement rate, kinematic states, and extension of the JDTC-PMBM-GGIW filter is smaller than that of JDTC-GIW-MeMBer filter and JDTC-GIW-PHD filter. This means that the proposed JDTC-PMBM-GGIW filter outperforms the JDTC-GIW-MeMBer filter and JDTC-GIW-PHD filter. Figure 4d indicates that the proposed JDTC-PMBM-GGIW filter is unbiased in terms of cardinality estimation. Figure 5 shows the class PMFs of the proposed JDTC-PMBM-GGIW filter, JDTC-GIW-MeMBer filter, and JDTC-GIW-PHD filter. The probabilities for the correct class of each EO estimated by the three methods exceed the decision threshold of 0.5. This means that these three methods can correctly classify EOs. As seen from Figure 5, the class probability mass function of the proposed JDTC-PMBM-GGIW method is more robust.

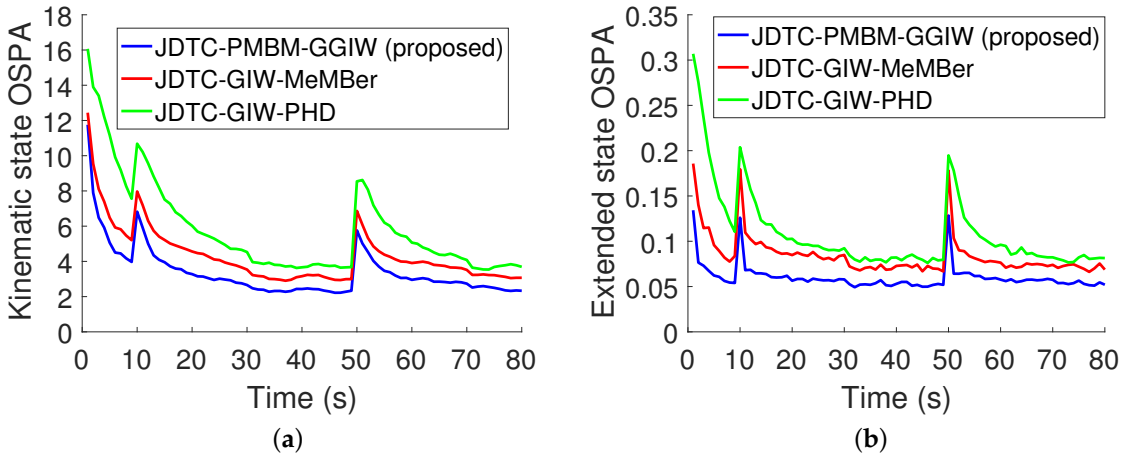

Figure 4. *Cont.*

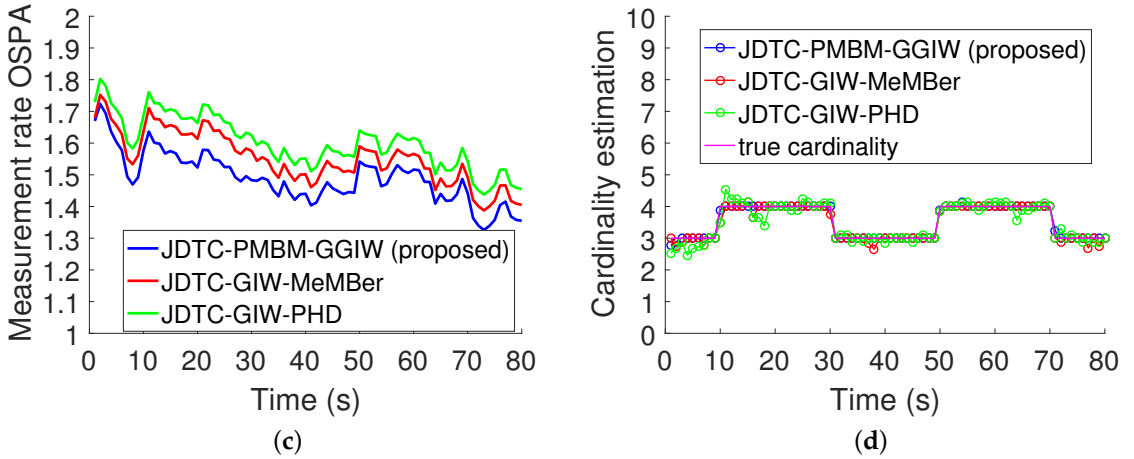

(**c**) (**d**)

Figure 4. Tracking performance comparison of three RFS-based multiple extended objects JDTC algorithms in scenario 1. (**a**) Kinematic state OSPA distance; (**b**) Extended state OSPA distance; (**c**) Measurement rate OSPA distance; (**d**) Cardinality estimation of the targets.

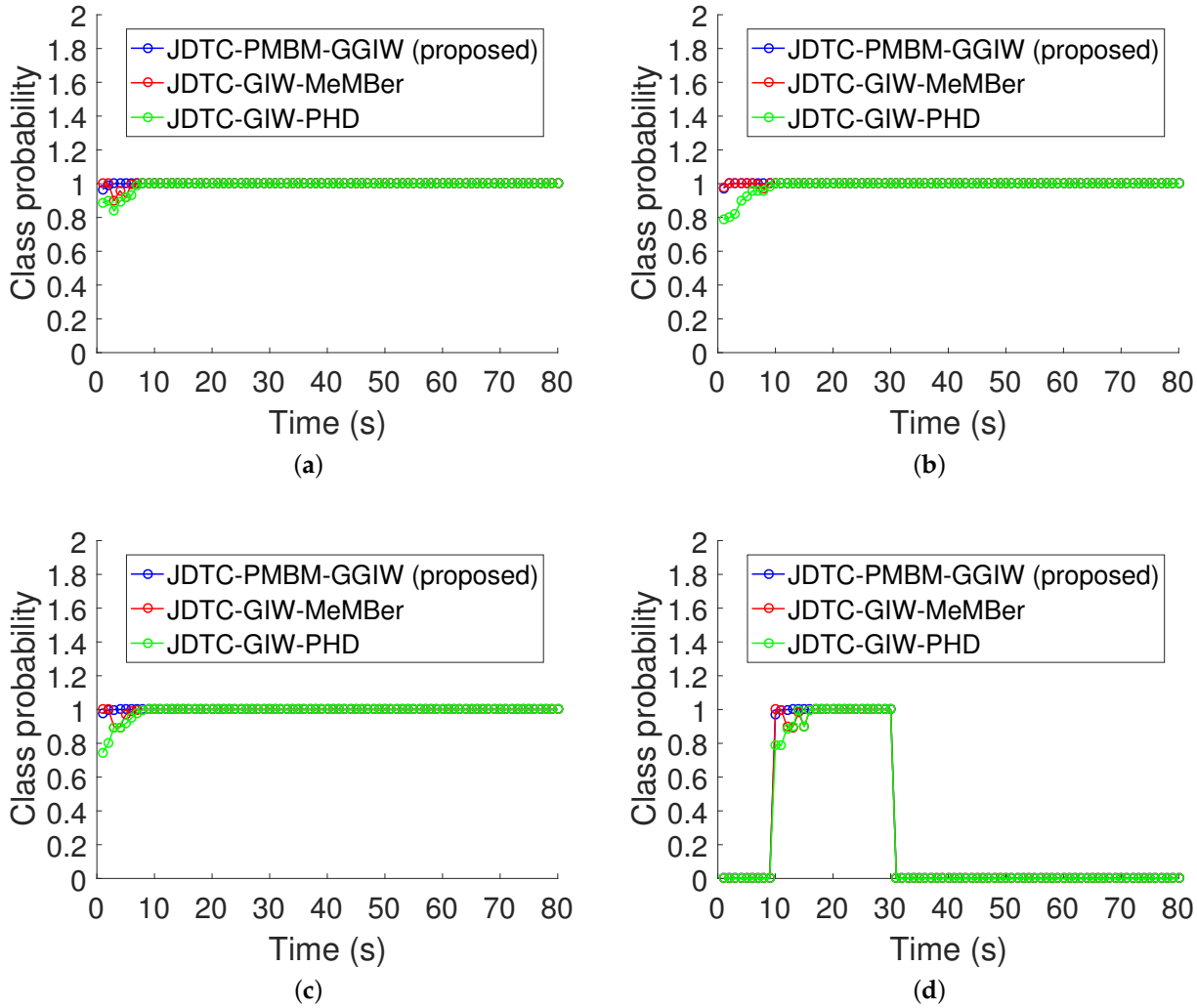

(**a**) (**b**)

(**c**) (**d**)

Figure 5. *Cont.*

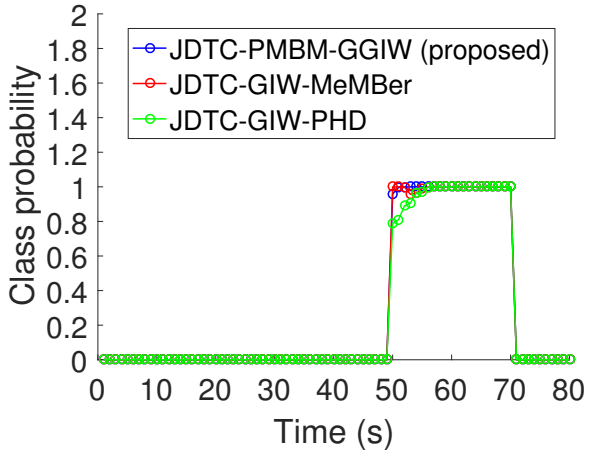

(**e**)

Figure 5. Classification performance comparison of three RFS-based multiple extended objects JDTC algorithms in scenario 1. (**a**) The class probability mass function of the correct class for EO 1; (**b**) The class probability mass function of the correct class for EO 2; (**c**) The class probability mass function of the correct class for EO 3; (**d**) The class probability mass function of the correct class for EO 4; (**e**) The class probability mass function of the correct class for EO 5.

6.3.2. Scenario 2

As can be seen in Figure 6a–c, the OSPA distance of measurement rate, kinematic states, and extension of the proposed JDTC-PMBM-GGIW filter is still lower overall than that of the JDTC-GIW-MeMBer filter and JDTC-GIW-PHD filter in the maneuvering scenario. Similar to the simulation results of scenario 1, Figure 6d indicates that the proposed JDTC-PMBM-GGIW filter is unbiased in terms of cardinality estimation. The class probability mass functions of each EO are shown in Figure 7, from which we can see that the probabilities of the correct class of each EO estimated by the proposed JDTC-PMBM-GGIW filter, JDTC-GIW- MeMBer filter, and JDTC-GIW-PHD filter exceed the decision threshold 0.5 during the entire monitoring period, while the class PMFs of the proposed JDTC-PMBM-GGIW method are more stable. The simulation results mean that the proposed JDTC-PMBM-GGIW filter is able to detect, track, and classify multiple extended objects simultaneously with more robust performance.

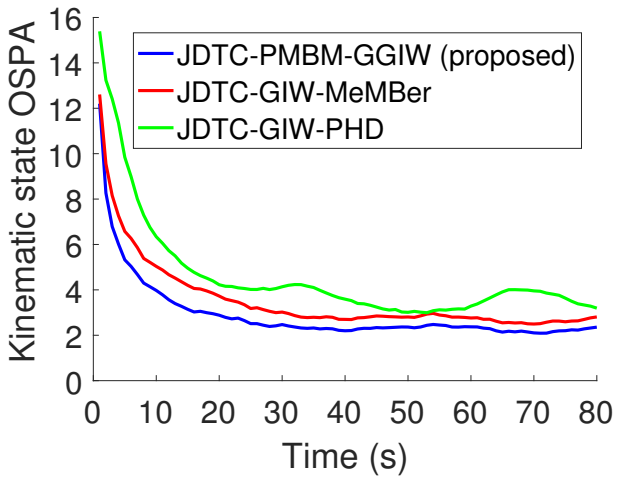

(**a**)

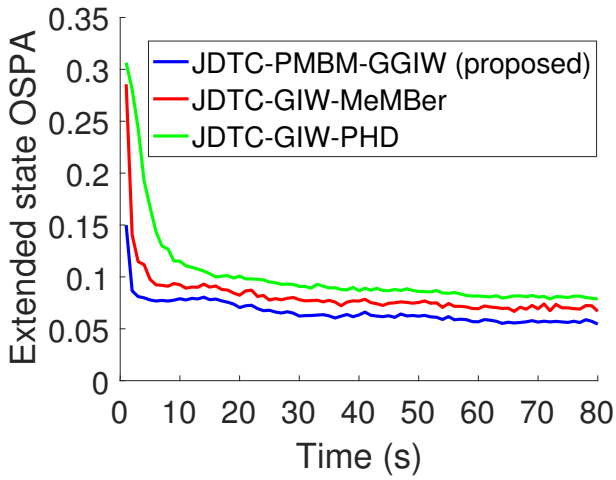

(**b**)

Figure 6. *Cont.*

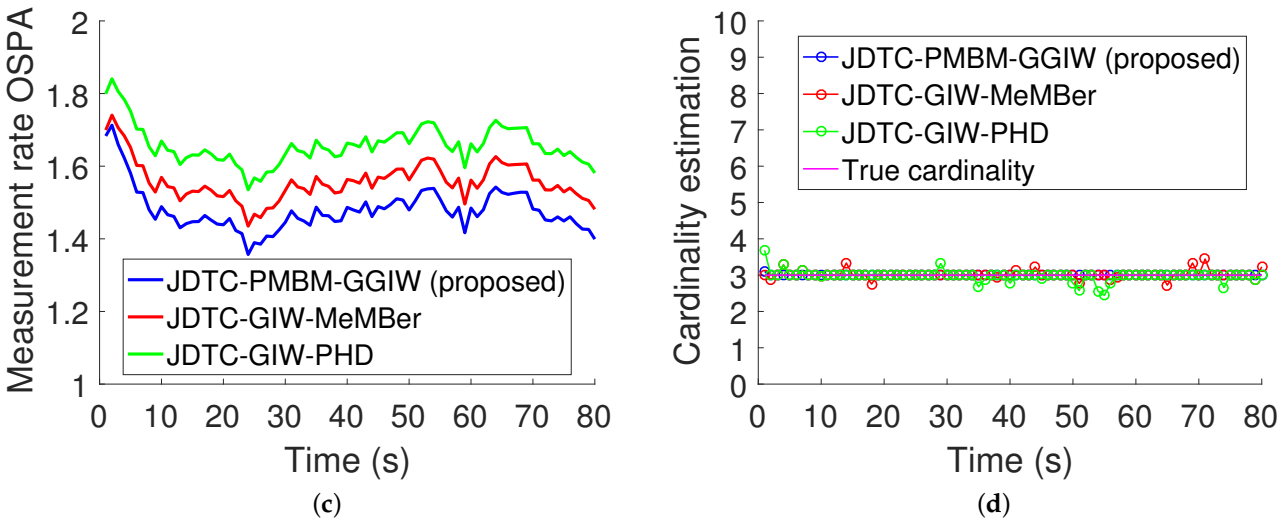

Figure 6. Tracking performance comparison of three RFS-based multiple extended objects JDTC algorithms in scenario 2. (**a**) Kinematic state OSPA distance; (**b**) Extended state OSPA distance; (**c**) Measurement rate OSPA distance; (**d**) Cardinality estimation of the targets.

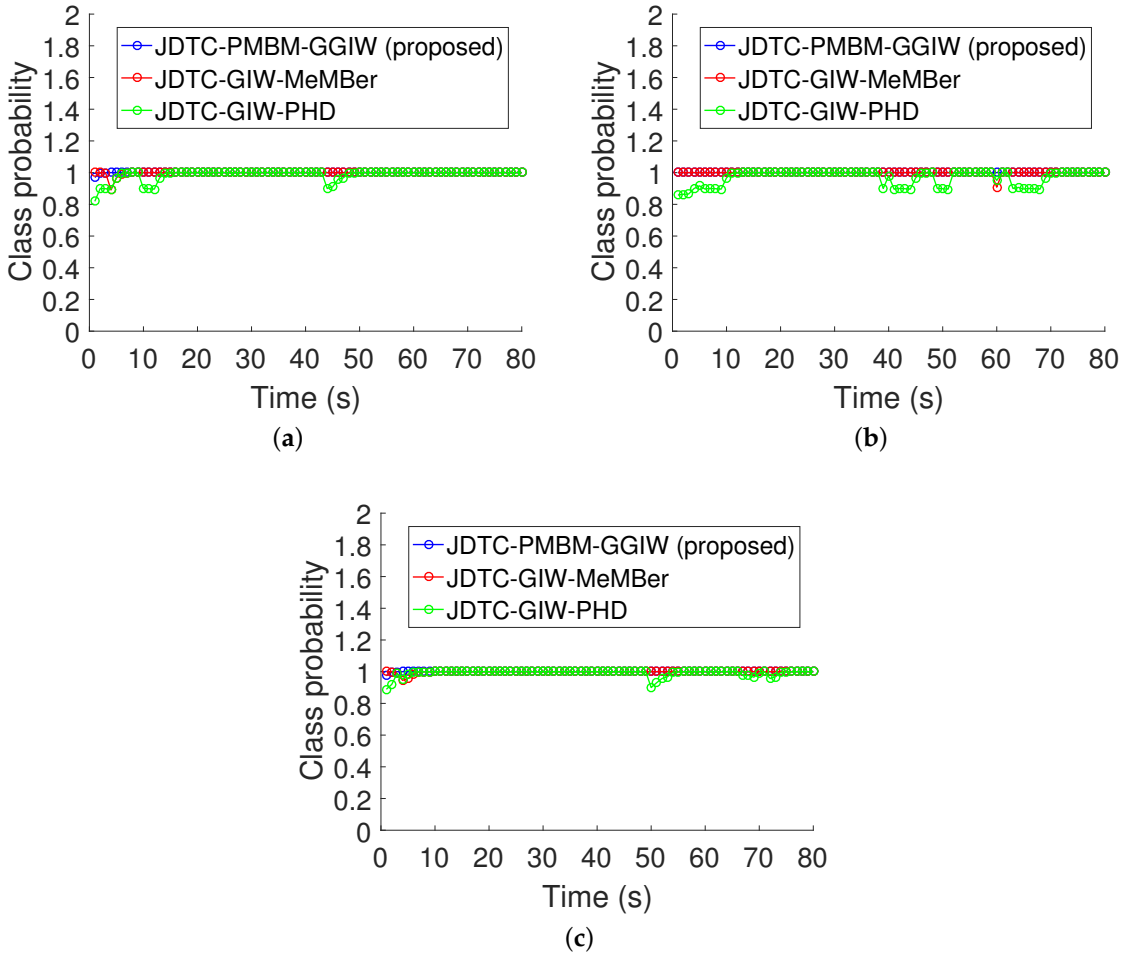

Figure 7. Classification performance comparison of three RFS-based multiple extended objects JDTC algorithms in scenario 2. (**a**) The class probability mass function of the correct class for EO 1; (**b**) The class probability mass function of the correct class for EO 2; (**c**) The class probability mass function of the correct class for EO 3.

6.3.3. The Average Execution Time

The average execution time of the three algorithms is reported in Table 5, from which we can see that the JDTC-GIW-MeMBer filter and JDTC-GIW-PHD filter run faster than the JDTC-PMBM-GGIW filter.

Table 5. The average execution time.

Algorithm	Scenario 1	Scenario 2
JDTC-PMBM-GGIW	16.59 s	8.89 s
JDTC-GIW-MeMBer	4.25 s	2.18 s
JDTC-GIW-PHD	4.01 s	1.94 s

6.3.4. Overall Performance Analysis

In Reference [35], we have analyzed and verified that the overall performance of the JDTC-GIW-MeMBer filter is better than that of the JDTC-GIW-PHD filter. In the simulation results of this paper, we can see that the JDTC performance of the proposed JDTC-PMBM-GGIW filter is obviously better than that of the JDTC-GIW-MeMBer filter. The reason for this is that the JDTC-GIW-MeMBer filter only propagates a single MB density, while the JDTC-PMBM-GGIW filter propagates a mixture density of multiple MB. Maintaining a single MB density propagation results in a larger OSPA distance. In addition, the JDTC-GIW-MeMBer algorithm does not satisfy the conjugate prior and ignores the problem of data association between the target and measurement. Therefore, the proposed JDTC-PMBM-GGIW filter in this paper achieves a good compromise in terms of JDTC performance and computation cost.

7. Discussion

As seen from the simulation results in Section 6.3, although the JDTC-PMBM filter has superior tracking and classification performance, the computation execution time is relatively long. The reason for this is that the number of data associations of the JDTC-PMBM filter grows dramatically in the update step. In order to further optimize the performance of the proposed JDTC-PMBM algorithm, in this section, we first analyze the computational complexity of the JDTC-PMBM algorithm and then discuss how to reduce the computational complexity.

7.1. Complexity

In this section, we discuss the number of possible data associations of the proposed JDTC-PMBM filter. Since the EO class directly corresponds to the pseudo-measurement, the association between the pseudo-measurement and the target class is unique. For the j-th predicted MB with the Bernoulli index set $\mathbb{I}^j$, the real measurements in $\mathbf{Z}^{r,k}$ can be assigned to $|\mathbb{I}^j|$ previously detected EOs or undetected EOs, or are identified as clutter. Thus, the number of possible associations can be derived by real measurement set partitions number and possible associations number for each partition. The number of elements in the partition cell of $\mathbf{Z}^{r,k}$ is between 1 and $|\mathbf{Z}^{r,k}|$. The number of possible partitions that partition the measurement set $\mathbf{Z}^{r,k}$ into C nonempty disjoint subsets can be expressed by the Stirling number of the second kind [47], i.e.,

$$\left\{ \begin{array}{c} |\mathbf{Z}^{r,k}| \\ C \end{array} \right\} = \frac{1}{C!} \sum_{j=0}^{C} (-1)^{C-j} \left(\begin{array}{c} C \\ j \end{array} \right) j^{|\mathbf{Z}^{r,k}|} \tag{99}$$

The size of the association space $\mathcal{A}^j$ is described as

$$N^{\mathcal{A}^j}\left(|\mathbf{Z}^{r,k}|, \left|\mathbb{I}^j\right|\right) = \sum_{C=1}^{|\mathbf{Z}^{r,k}|} \left\{ \begin{array}{c} |\mathbf{Z}^{r,k}| \\ C \end{array} \right\} \sum_{T=0}^{\min(C,|\mathbb{I}^j|)} \left(\begin{array}{c} C \\ T \end{array} \right) \frac{\left|\mathbb{I}^j\right|!}{\left(\left|\mathbb{I}^j\right| - T\right)!} \tag{100}$$

where the Binomial coefficient $\begin{pmatrix} C \\ T \end{pmatrix} = \frac{C!}{T!(C-T)!}$. Thus, for a predicted JDTC-PMBM with the space of global hypothesis $\mathbb{J}$, the number of possible associations is given by

$$N^{\mathcal{A}} = \sum_{j \in \mathbb{J}} N^{\mathcal{A}^j} \left(|\mathbf{Z}^{r,k}|, \left| \mathbb{I}^j \right| \right) \tag{101}$$

By recursively analyzing Equation (100), another expression of the total number of global hypotheses (MBs in the MBM) can be obtained at time k. Specifically, given a series of real measurement sets from the beginning time to including the time step k, and the initial MBM is empty, the number of MBs components in the updated JDTC-PMBM density at time step k can be described as the Bell number whose order n is the sum of the number of measurements in all received measurement sets, i.e.,

$$\left| \mathbb{J}_{k|k} \right| = B\left(\sum_{t=1}^{k} \left| \mathbf{Z}^{r,t} \right| \right) = B(|\cup_{t=1}^{k} \mathbf{Z}^{r,t}|) \tag{102}$$

where $B(n)$ denotes the Bell number of n:th order.

7.2. Complexity Reduction and State Extraction

According to the analysis in Section 7.1, the number of associations of the proposed JDTC-PMBM-GGIW algorithm increases rapidly during the iterative update process. In order to reduce the computation time cost of the proposed JDTC-PMBM-GGIW algorithm, we need to consider reducing the number of associations and JDTC-PMBM components.

For the reduction of the number of associations, gating [48,49], partitioning [17,50–52], and assignment using Murty's algorithm [53] are executed. After performing the three step procedures, a subset of associations is generated and the number of associations in the updated JDTC-PMBM-GGIW algorithm is drastically reduced. For the MBs components reduction in MBM, MBs whose updated weights are lower than the preset threshold will be pruned from the MBM. In addition, if the upper bound of Kullback–Leibler divergence (KL-div) of two MBs is smaller than a preset threshold, two MBs can be merged [32,54]. For the Bernoullis components reduction, if the existence probability of the Bernoulli is lower than the preset threshold, the Bernoulli component is removed from the MB.

For the PPP intensity expressed as a mixture distribution, the mixture component is removed if its weight is less than a preset threshold. Additionally, minimizing KL-div method can also be used to merge two or more similar mixture components.

For the GGIW components reduction, the pruning and merging operations described in References [17,26,35] are used to reduce the number of GGIW components.

Finally, we choose the largest weight MB in MBM. If the existence probability of Bernoulli components and class probability simultaneously exceed the threshold, the EO state extraction based on the maximum a posterior (MAP) criterion is implemented [35].

8. Conclusions

This paper extends the Poisson multi-Bernoulli mixture (PMBM) filter to implement joint detection, tracking, and classification (JDTC) of multiple extended objects (EOs). More specifically, for the EOs with elliptic shapes, the update and the prediction equations of the PMBM filter for JDTC problem are established, and class PMF is derived. Then, the analytical and closed implementation process based on the product of a gamma-Gaussian-Inverse-Wishart (GGIW) distribution and class probability mass function (PMF) is derived. Finally, according to the estimated GGIW parameters, the kinematic state, extended state, Poisson measurement rate, and the class probability of each EO at each time are extracted. The effectiveness of the proposed JDTC-PMBM-GGIW algorithm is verified by simulation experiments in two scenarios. The performance graphs in the simulation results show that the performance of the proposed JDTC-PMBM-GGIW algorithm is better than that of the JDTC-GIW-MeMBer algorithm and JDTC-GIW-PHD algorithm in measurement

rate estimation, kinematic states estimation, extension estimation, and class probability estimation. In addition, we also discuss the computational complexity and the average running time of the proposed JDTC-PMBM-GGIW algorithm, and give the corresponding methods to reduce the computational complexity. In conclusion, the proposed JDTC-PMBM-GGIW algorithm achieves a good compromise in computational complexity and JDTC performance.

In the future, the JDTC performance of the JDTC-PMBM algorithm with arbitrary shape EOs in complex scenes will be further evaluated. Indeed, the proposed JDTC-PMBM algorithm in this paper can be extended to the JDTC problem of EOs with arbitrary shapes. In this case, it is needed to construct new pseudo-measurement likelihood functions and new classification criteria. In addition, we will perform experiments on real-world datasets to further evaluate the availability, effectiveness, and robustness of the proposed JDTC-PMBM-GGIW algorithm.

Author Contributions: Conceptualization, Y.L. and M.Y.; Formal analysis, Y.L.; Funding acquisition, P.W. and H.Z.; Methodology, Y.W.; Software, Y.L. and P.W.; Supervision, H.Z.; Writing— original draft, Y.L.; Writing—review and editing, P.W. and Y.W. All authors have read and agreed to the published version of the manuscript.

Funding: This work was supported by the National Natural Science Foundation of China under grants No. 61971103 and No. 62101112, and the Science and Technology on Electronic Information Control Laboratory (NO. 6142105190307).

Data Availability Statement: Data sharing not applicable. No new data were created or analyzed in this study. Data sharing is not applicable to this article.

Conflicts of Interest: The authors declare no conflict of interest.

Abbreviations

Abbreviations Table and Main Symbols Table

Abbreviations	**Full Name**
RFS	Random Finite Set
PHD	Probability Hypothesis Density
CPHD	Cardinalized Probability Hypothesis Density
GIW	Gaussian Inverse Wishart
GGIW	Gamma Gaussian Inverse Wishart
GLMB	Generalized Labeled Multi-Bernoulli
MB	Multi-Bernoulli
SPD	Symmetric Positive Define
MBM	Multi-Bernoulli Mixture
MR	Measurement Rate
PPP	Poisson Point Process
PMBM	Poisson Multi-Bernoulli Mixture
JDTC	Joint Detection, Tracking and Classification
PMF	Probability Mass Function
EOs	Extended Objects
OSPA	Optimal Sub-Pattern Assignment
PDF	Probability Density Function
Symbols	**Description**
$\mathbf{x}_k$	Kinematic state
$\mathbf{X}_k$	Extended state
γ_k	Poisson measurement rate of an EO
$\mathcal{C}_k^c$	Class of an EO
n_c	The total number of categories for EOs
$\mathbf{X}_k$	Generalized Labeled Multi-Bernoulli
$\mathbf{E}_k^c$	Direction matrix of an EO

$\mathbf{Z}_k^{p,c}$	Scale matrix of the c-th EO; Pseudo measurement
$\mathcal{PS}(\cdot)$	Poisson distribution
$\mathcal{W}(\cdot)$	Wishart distribution
$\mathcal{N}(\cdot)$	Gaussian distribution
$\mathcal{GAM}(\cdot)$	Gamma distribution
$\mathcal{IW}(\cdot)$	Inverse Wishart distribution
$\mathbf{C}_c$	The real measurement set corresponding to the target
$\psi_{\mathbf{C}_c}(\cdot)$	The likelihood function corresponding to measurement set $\mathbf{C}_c$
$\psi_{\mathbf{Z}_k^{p,c}}(\cdot)$	The pseudo measurement likelihood function
$\mathbf{Z}^{r,k}$	The received real measurement set
$\mathcal{A}^j$	The j-th predicted global hypothesis index space
$\mathbb{I}^j$	The target index space in the j-th global hypothesis
$\mathbb{M}$	The index space of real measurement
$D^u(\cdot)$	The intensity function of a PPP
$r_k^{j,i}$	The existence probability of the i-th Bernoulli in the j-th global hypothesis
$f^{j,i}(\cdot)$	The spatial PDF of the i-th Bernoulli in the j-th global hypothesis
$\mathcal{W}_k^j$	The weight of the j-th MB

Appendix A. Proof of the Class PMF

We define $p(\mathbf{Z}_k|\mathcal{C}_k^c, \xi_k, \mathbf{Z}^{k-1}) = \psi_{\mathbf{C}_c}(\mathbf{y}_k)\psi_{\mathbf{Z}_k^{p,c}}(\mathbf{y}_k)$, then,

$$\frac{p(\mathcal{C}_k^c|\mathbf{Z}^{k-1})\int \psi_{\mathbf{C}_c}(\mathbf{y}_k)\psi_{\mathbf{Z}_k^{p,c}}(\mathbf{y}_k)f_+(\xi_k|\mathcal{C}_k^c,\mathbf{Z}^{k-1})d\xi_k}{\sum_{c=1}^{n_c} p(\mathcal{C}_k^c|\mathbf{Z}^{k-1})\int \psi_{\mathbf{C}_c}(\mathbf{y}_k)\psi_{\mathbf{Z}_k^{p,c}}(\mathbf{y}_k)f_+(\xi_k|\mathcal{C}_k^c,\mathbf{Z}^{k-1})d\xi_k} \tag{A1}$$

$$\begin{aligned}
&= \frac{p(\mathcal{C}_k^c|\mathbf{Z}^{k-1})\int p(\mathbf{Z}_k|\mathcal{C}_k^c,\xi_k,\mathbf{Z}^{k-1})f_+(\xi_k|\mathcal{C}_k^c,\mathbf{Z}^{k-1})d\xi_k}{\sum_{c=1}^{n_c} p(\mathcal{C}_k^c|\mathbf{Z}^{k-1})\int p(\mathbf{Z}_k|\mathcal{C}_k^c,\xi_k,\mathbf{Z}^{k-1})f_+(\xi_k|\mathcal{C}_k^c,\mathbf{Z}^{k-1})d\xi_k} \\
&= \frac{p(\mathbf{Z}_k|\mathcal{C}_k^c,\mathbf{Z}^{k-1})p(\mathcal{C}_k^c|\mathbf{Z}^{k-1})}{p(\mathbf{Z}_k|\mathbf{Z}^{k-1})} \\
&= p(\mathcal{C}_k^c|\mathbf{Z}^k)
\end{aligned} \tag{A2}$$

Appendix B. Proof of the Update JDTC-PMBM-GGIW Parameters

According to Section 4.3, for a predicted density $f_+(\xi_k, \mathcal{C}_k^c|\mathbf{Z}^{k-1})$, we have the update:

$$\begin{aligned}
f_{\mathbf{C}_c}(\mathbf{y}_k|\mathbf{Z}^k) &= \frac{\psi_{\mathbf{C}_c}(\mathbf{y}_k)\psi_{\mathbf{Z}_k^{p,c}}(\mathbf{y}_k)f_+(\xi_k,\mathcal{C}_k^c|\mathbf{Z}^{k-1})}{\left\langle f_+(\xi_k,\mathcal{C}_k^c|\mathbf{Z}^{k-1});\psi_{\mathbf{C}_c}(\mathbf{y}_k)\psi_{\mathbf{Z}_k^{p,c}}(\mathbf{y}_k)\right\rangle} \\
&= \frac{p(\mathcal{C}_k^c|\mathbf{Z}^{k-1})\psi_{\mathbf{C}_c}(\mathbf{y}_k)\psi_{\mathbf{Z}_k^{p,c}}(\mathbf{y}_k)f_+(\xi_k|\mathcal{C}_k^c,\mathbf{Z}^{k-1})}{p(\mathcal{C}_k^c|\mathbf{Z}^{k-1})\int \psi_{\mathbf{C}_c}(\mathbf{y}_k)\psi_{\mathbf{Z}_k^{p,c}}(\mathbf{y}_k)f_+(\xi_k|\mathcal{C}_k^c,\mathbf{Z}^{k-1})d\xi_k} \\
&\times \frac{p(\mathcal{C}_k^c|\mathbf{Z}^{k-1})\int \psi_{\mathbf{C}_c}(\mathbf{y}_k)\psi_{\mathbf{Z}_k^{p,c}}(\mathbf{y}_k)f_+(\xi_k|\mathcal{C}_k^c,\mathbf{Z}^{k-1})d\xi_k}{\sum_{c=1}^{n_c} p(\mathcal{C}_k^c|\mathbf{Z}^{k-1})\int \psi_{\mathbf{C}_c}(\mathbf{y}_k)\psi_{\mathbf{Z}_k^{p,c}}(\mathbf{y}_k)f_+(\xi_k|\mathcal{C}_k^c,\mathbf{Z}^{k-1})d\xi_k}
\end{aligned} \tag{A3}$$

$$= f_{\mathbf{C}_c}(\xi_k|\mathcal{C}_k^c,\mathbf{Z}^k)p(\mathcal{C}_k^c|\mathbf{Z}^k) \tag{A4}$$

where $f_+(\xi_k|\mathcal{C}_k^c,\mathbf{Z}^{k-1})$ is the predicted density of the c-th class target.

Since the measurement rate $\gamma_k(\xi_k, \mathcal{C}_k^c)$ in (5) is unknown at time k, it is approximately replaced by $\gamma_{k|k-1}$, and $\gamma_{k|k-1}$ can be obtained in the predicted step. Firstly, the product of the likelihood function $\psi_{\mathbf{C}_c}(\mathbf{y}_k)$ and $\psi_{\mathbf{Z}_k^{p,c}}(\mathbf{y}_k)$ is given by

$$\begin{aligned}\psi_{\mathbf{C}_c}(\mathbf{y}_k)\psi_{\mathbf{Z}_k^{p,c}}(\mathbf{y}_k) &= \mathcal{PS}(|\mathbf{C}_c|;\gamma_{k|k-1})p_D(\mathbf{y}_k)e^{-\gamma_{k|k-1}}(\gamma_{k|k-1})^{|\mathbf{C}_c|}L_{\mathbf{C}_c} \\ &\times \mathcal{N}(\bar{\mathbf{z}}_k^{\mathbf{C}_c};(\mathbf{H}_k)\mathbf{x}_k, \frac{\mathbf{R}_k+\eta\mathbf{X}_k}{|\mathbf{C}_c|})\mathcal{W}(\mathbf{Z}_k^{p,c};\delta_k^{p,c}, \mathbf{E}_k^c\mathbf{X}_k(\mathbf{E}_k^c)^\top/\delta_k^{p,c})\end{aligned} \tag{A5}$$

where

$$L_{k,\mathbf{C}_c} = (2\pi)^{\frac{-(|\mathbf{C}_c|-1)d}{2}}|\mathbf{R}_k+\eta\mathbf{X}_k|^{\frac{-(|\mathbf{C}_c|-1)}{2}}|\mathbf{C}_c|^{\frac{-d}{2}}\,\mathrm{etr}(-\frac{1}{2}\mathbf{Z}_k^{\mathbf{C}_c}(\mathbf{R}_k+\eta\mathbf{X}_k)^{-1}) \tag{A6}$$

$$\bar{\mathbf{z}}_k^{\mathbf{C}_c} = \frac{1}{|\mathbf{C}_c|}\sum_{j=1}^{|\mathbf{C}_c|}\mathbf{z}_j^{\mathbf{C}_c} \tag{A7}$$

$$\mathbf{Z}_k^{\mathbf{C}_c} \triangleq \sum_{j=1}^{|\mathbf{C}_c|}(\mathbf{z}_j^{\mathbf{C}_c}-\bar{\mathbf{z}}_k^{\mathbf{C}_c})(\mathbf{z}_j^{\mathbf{C}_c}-\bar{\mathbf{z}}_k^{\mathbf{C}_c})^\top \tag{A8}$$

According to the Cholesky Factorization [7], the noise covariance of real measurements $\mathbf{R}_k+\eta\mathbf{X}_k$ in (6) is approximately computed by

$$(\mathbf{R}_k+\eta\mathbf{X}_k) \approx \mathbf{B}_k\mathbf{X}_k(\mathbf{B}_k)^\top \tag{A9}$$

where $\mathbf{B}_k = (\mathbf{R}_k+\eta\overline{\mathbf{X}}_{k|k-1})^{1/2}(\overline{\mathbf{X}}_{k|k-1})^{-1/2}$. $\overline{\mathbf{X}}_{k|k-1}$ can be obtained via the prediction results.

The predicted density of the c-th class EO is described as a GGIW distribution, i.e.,

$$f_+(\xi_k|\mathcal{C}_k^c, \mathbf{Z}^{k-1}) = \mathcal{GAM}(\gamma_k;\alpha_{k|k-1}^c,\beta_{k|k-1}^c)\mathcal{N}(\mathbf{x}_k;\mathbf{m}_{k|k-1}^c,\mathbf{P}_{k|k-1}^c)\mathcal{IW}(\mathbf{X}_k;v_{k|k-1}^c,\mathbf{V}_{k|k-1}^c) \tag{A10}$$

Next, we compute the product of $f_+(\xi_k|\mathcal{C}_k^c, \mathbf{Z}^{k-1})$ and $\psi_{\mathbf{C}_c}(\mathbf{y}_k)\psi_{\mathbf{Z}_k^{p,c}}(\mathbf{y}_k)$, i.e.,

$$\begin{aligned}&\mathcal{PS}(|\mathbf{C}_c|;\gamma_{k|k-1})p_D(\mathbf{y}_k)e^{-\gamma_{k|k-1}}(\gamma_{k|k-1})^{|\mathbf{C}_c|}L_{k,\mathbf{C}_c} \\ &\times \mathcal{N}(\bar{\mathbf{z}}_k^{\mathbf{C}_c};(\mathbf{H}_k)\mathbf{x}_k, \frac{\mathbf{R}_k+\eta\overline{\mathbf{X}}_{k|k-1}}{|\mathbf{C}_c|})\mathcal{W}(\mathbf{Z}_k^{p,c};\delta_k^{p,c}, \mathbf{E}_k^c\overline{\mathbf{X}}_{k|k-1}(\mathbf{E}_k^c)^\top/\delta_k^{p,c}) \\ &\mathcal{GAM}(\gamma_k;\alpha_{k|k-1}^c,\beta_{k|k-1}^c)\mathcal{N}(\mathbf{x}_k;\mathbf{m}_{k|k-1}^c,\mathbf{P}_{k|k-1}^c)\mathcal{IW}(\mathbf{X}_k;v_{k|k-1}^c,\mathbf{V}_{k|k-1}^c)\end{aligned} \tag{A11}$$

We define $Q_k^{c,\mathbf{C}_c} \triangleq p_D(\mathbf{y}_k)e^{-\gamma_{k|k-1}}(\gamma_{k|k-1})^{|\mathbf{C}_c|}$.
For the γ part update,

$$\begin{aligned}&\mathcal{PS}(|\mathbf{C}_c|;\gamma_{k|k-1}^c)\mathcal{GAM}(\gamma_k;\alpha_{k|k-1}^c,\beta_{k|k-1}^c) \\ &= \frac{\Gamma(\alpha_{k|k-1}^c+|\mathbf{C}_c|)(\beta_{k|k-1}^c)^{\alpha_{k|k-1}^c}}{\Gamma(\alpha_{k|k-1}^c)(\beta_{k|k-1}^c+1)^{\alpha_{k|k-1}^c+|\mathbf{C}_c|}|\mathbf{C}_c|!} \\ &\quad\times \mathcal{GAM}(\gamma_k;\alpha_k^{c,\mathbf{C}_c},\beta_k^{c,\mathbf{C}_c})\end{aligned} \tag{A12}$$

$$\triangleq G_k^{c,\mathbf{C}_c}\mathcal{GAM}(\gamma_k;\alpha_k^{c,\mathbf{C}_c},\beta_k^{c,\mathbf{C}_c}) \tag{A13}$$

where

$$\alpha_k^{c,\mathbf{C}_c} = \alpha_{k|k-1}^c + |\mathbf{C}_c| \tag{A14}$$

$$\beta_k^{c,\mathbf{C}_c} = \beta_{k|k-1}^c + 1 \tag{A15}$$

Since

$$\begin{aligned}&\mathcal{N}(\bar{\mathbf{z}}_k^{\mathbf{C}_c};(\mathbf{H}_k)\mathbf{x}_k,\frac{\mathbf{R}_k+\eta\overline{\mathbf{X}}_{k|k-1}}{|\mathbf{C}_c|})\mathcal{N}(\mathbf{x}_{k|k-1};\mathbf{m}_{k|k-1}^c,\mathbf{P}_{k|k-1}^c)\\&=\mathcal{N}(\bar{\mathbf{z}}_k^{\mathbf{C}_c};(\mathbf{H}_k)\mathbf{m}_{k|k-1}^c,\mathbf{S}_{k|k-1}^{c,\mathbf{C}_c})\mathcal{N}(\mathbf{x}_k;\mathbf{m}_k^{c,\mathbf{C}_c},\mathbf{P}_k^{c,\mathbf{C}_c})\end{aligned}\tag{A16}$$

where

$$\mathbf{S}_{k|k-1}^{c,\mathbf{C}_c}=\mathbf{H}_k\mathbf{P}_{k|k-1}^c(\mathbf{H}_k)^\top+\frac{\mathbf{B}_k\overline{\mathbf{X}}_{k|k-1}(\mathbf{B}_k)^\top}{|\mathbf{C}_c|}\tag{A17}$$

$$K_{k|k-1}^{(c,\mathbf{C}_c)}=\mathbf{P}_{k|k-1}^c(\mathbf{H}_k)^\top(\mathbf{S}_{k|k-1}^{c,\mathbf{C}_c})^{-1}\tag{A18}$$

$$\varepsilon_{k|k-1}^{(c,\mathbf{C}_c)}=\bar{\mathbf{z}}_k^{\mathbf{C}_c}-(\mathbf{H}_k)\mathbf{m}_{k|k-1}^c\tag{A19}$$

$$\mathbf{m}_k^{c,\mathbf{C}_c}=\mathbf{m}_{k|k-1}^c+(K_{k|k-1}^{(c,\mathbf{C}_c)})\varepsilon_{k|k-1}^{(c,\mathbf{C}_c)}\tag{A20}$$

$$\mathbf{P}_k^{c,\mathbf{C}_c}=\mathbf{P}_{k|k-1}^c-K_{k|k-1}^{(c,\mathbf{C}_c)}\mathbf{H}_k\mathbf{P}_{k|k-1}^c\tag{A21}$$

Then, the rest of (A11)

$$\mathcal{N}(\bar{\mathbf{z}}_k^{\mathbf{C}_c};(\mathbf{H}_k)\mathbf{m}_{k|k-1}^c,\mathbf{S}_{k|k-1}^{c,\mathbf{C}_c})\mathcal{IW}(\mathbf{X}_{k|k-1};v_{k|k-1}^c,\mathbf{V}_{k|k-1}^c)L_{k,\mathbf{C}_c}\mathcal{W}(\mathbf{Z}_k^{p,c};\delta_k^{p,c},\mathbf{E}_k^c\overline{\mathbf{X}}_{k|k-1}(\mathbf{E}_k^c)^\top/\delta_k^{p,c})\tag{A22}$$

can be described as (A23),

$$\begin{aligned}&\mathcal{N}(\bar{\mathbf{z}}_k^{\mathbf{C}_c};(\mathbf{H}_k)\mathbf{m}_{k|k-1}^c,\mathbf{S}_{k|k-1}^{c,\mathbf{C}_c})\mathcal{IW}(\mathbf{X}_{k|k-1};v_{k|k-1}^c,\mathbf{V}_{k|k-1}^c)L_{k,\mathbf{C}_c}\mathcal{W}(\mathbf{Z}_k^{p,c};\delta_k^{p,c},\mathbf{E}_k^c\overline{\mathbf{X}}_{k|k-1}(\mathbf{E}_k^c)^\top/\delta_k^{p,c})\\&=\frac{2^{\frac{(|\mathbf{C}_c|+\delta_k^{p,c})(1-d)}{2}}|\mathbf{Z}_k^{p,c}|^{\frac{\delta_k^{p,c}-d-1}{2}}|\delta_k^{p,c}|^{\frac{\delta_k^{p,c}}{2}}}{\pi^{\frac{(|\mathbf{C}_c|d)}{2}}(|\mathbf{C}_c|)^{\frac{d}{2}}|\mathbf{B}_k|^{|\mathbf{C}_c|-1}|\mathbf{S}_{k|k-1}^{c,\mathbf{C}_c}(\overline{\mathbf{X}}_{k|k-1})^{-1}|^{\frac{1}{2}}}\frac{|\mathbf{V}_{k|k-1}^c|^{\frac{v_{k|k-1}^c-d-1}{2}}}{|\mathbf{V}_k^{c,\mathbf{C}_c}|^{\frac{v_{k|k-1}^c+|\mathbf{C}_c|+\delta_k^{p,c}-d-1}{2}}}\\&\quad\times\frac{\Gamma_d(\frac{v_{k|k-1}^c+|\mathbf{C}_c|+\delta_k^{p,c}-d-1}{2})}{\Gamma_d(\frac{v_{k|k-1}^c-d-1}{2})\Gamma_d(\frac{\delta_k^{p,c}}{2})}\mathcal{IW}(\mathbf{X}_k;v_k^{c,\mathbf{C}_c},\mathbf{V}_k^{c,\mathbf{C}_c})\end{aligned}\tag{A23}$$

$$\triangleq\Delta_k^{c,\mathbf{C}_c}\mathcal{IW}(\mathbf{X}_k;v_k^{c,\mathbf{C}_c},\mathbf{V}_k^{c,\mathbf{C}_c})\tag{A24}$$

where

$$\varepsilon_{k|k-1}^{(c,\mathbf{C}_c)}=\bar{\mathbf{z}}_k^{\mathbf{C}_c}-(\mathbf{H}_k)\mathbf{m}_{k|k-1}^c\tag{A25}$$

$$v_k^{c,\mathbf{C}_c}=v_{k|k-1}^c+|\mathbf{C}_c|+\delta_k^{p,c}\tag{A26}$$

$$\mathbf{V}_k^{c,\mathbf{C}_c}=\mathbf{V}_{k|k-1}^c+\mathbf{N}_k^{c,\mathbf{C}_c}+(\mathbf{B}_k)^{-1}\mathbf{Z}_k^{\mathbf{C}_c}(\mathbf{B}_k)^{-\top}+\delta_k^{p,c}(\mathbf{E}_k^c)^{-1}\mathbf{Z}_k^{p,c}(\mathbf{E}_k^c)^{-\top}\tag{A27}$$

$$\mathbf{N}_k^{c,\mathbf{C}_c}=\varepsilon_{k|k-1}^{(c,\mathbf{C}_c)}(\varepsilon_{k|k-1}^{(c,\mathbf{C}_c)})^\top(\mathbf{S}_{k|k-1,j}^{c,\mathbf{C}_c})^{-1}\overline{\mathbf{X}}_{k|k-1}\tag{A28}$$

By combining (A13), (A16), (A23), then (A11) can be obtained as GGIW form, i.e.,

$$\begin{aligned}&\psi_{\mathbf{C}_c}(\mathbf{y}_k)\psi_{\mathbf{Z}_k^{p,c}}(\mathbf{y}_k)f_+(\xi_k|\mathcal{C}_k^c,\mathbf{Z}^{k-1})\\&=Q_k^{c,\mathbf{C}_c}G_k^{c,\mathbf{C}_c}\Delta_k^{c,\mathbf{C}_c}\mathcal{GAM}(\gamma_k;\alpha_k^{c,\mathbf{C}_c},\beta_k^{c,\mathbf{C}_c})\mathcal{N}(\mathbf{x}_k;\mathbf{m}_k^{c,\mathbf{C}_c},\mathbf{P}_k^{c,\mathbf{C}_c})\mathcal{IW}(\mathbf{X}_k;v_k^{c,\mathbf{C}_c},\mathbf{V}_k^{c,\mathbf{C}_c})\end{aligned}\tag{A29}$$

According to Appendix A, the class probability mass function is given by

$$\begin{aligned} p(\mathcal{C}_k^c|\mathbf{Z}^k) &= \frac{p(\mathcal{C}_k^c|\mathbf{Z}^{k-1}) \int \psi_{\mathbf{C}_c}(\mathbf{y}_k)\psi_{\mathbf{Z}_k^{p,c}}(\mathbf{y}_k) f_+(\xi_k|\mathcal{C}_k^c, \mathbf{Z}^{k-1}) d\xi_k}{\sum_{c=1}^{n_c} p(\mathcal{C}_k^c|\mathbf{Z}^{k-1}) \int \psi_{\mathbf{C}_c}(\mathbf{y}_k)\psi_{\mathbf{Z}_k^{p,c}}(\mathbf{y}_k) f_+(\xi_k|\mathcal{C}_k^c, \mathbf{Z}^{k-1}) d\xi_k} \\ &= \frac{p(\mathcal{C}_k^c|\mathbf{Z}^{k-1}) Q_k^{c,\mathbf{C}_c} G_k^{c,\mathbf{C}_c} \Delta_k^{c,\mathbf{C}_c}}{\sum_{c=1}^{n_c} p(\mathcal{C}_k^c|\mathbf{Z}^{k-1}) Q_k^{c,\mathbf{C}_c} G_k^{c,\mathbf{C}_c} \Delta_k^{c,\mathbf{C}_c}} \end{aligned} \tag{A30}$$

Thus, given the predicted spatial density $f_+^{j,i_C}(\mathbf{y}_k)$ of the i_C-th Bernoulli of the j-th MB component, the updating spatial density $f_{\mathbf{C}_c}^{j,i_C}(\mathbf{y}_k|\mathbf{Z}^k)$ is given by

$$\begin{aligned} f_{\mathbf{C}_c}^{j,i_C}(\mathbf{y}_k|\mathbf{Z}^k) &= \frac{\psi_{\mathbf{C}_c}(\mathbf{y}_k)\psi_{\mathbf{Z}_k^{p,c}}(\mathbf{y}_k) f_+^{j,i_C}(\xi_k, \mathcal{C}_k^c|\mathbf{Z}^{k-1})}{\left\langle f_+^{j,i_C}(\xi_k, \mathcal{C}_k^c|\mathbf{Z}^{k-1}); \psi_{\mathbf{C}_c}(\mathbf{y}_k)\psi_{\mathbf{Z}_k^{p,c}}(\mathbf{y}_k) \right\rangle} \\ &= \frac{\mu_{j,i_C,k|k-1}^c Q_k^{c,\mathbf{C}_c} G_k^{c,\mathbf{C}_c} \Delta_k^{c,\mathbf{C}_c}}{\sum_{c=1}^{n_c} \mu_{j,i_C,k|k-1}^c Q_k^{c,\mathbf{C}_c} G_k^{c,\mathbf{C}_c} \Delta_k^{c,\mathbf{C}_c}} \mathcal{GAM}(\gamma_k; \alpha_{j,i_C,k}^{c,\mathbf{C}_c}, \beta_{j,i_C,k}^{c,\mathbf{C}_c}) \\ &\times \mathcal{N}(\mathbf{x}_k; \mathbf{m}_{j,i_C,k}^{c,\mathbf{C}_c}, \mathbf{P}_{j,i_C,k}^{c,\mathbf{C}_c}) \mathcal{IW}(\mathbf{X}_k; v_{j,i_C,k}^{c,\mathbf{C}_c}, \mathbf{V}_{j,i_C,k}^{c,\mathbf{C}_c}) \qquad \text{(A31)} \\ &= \mu_{j,i_C,k}^{c,\mathbf{C}_c} \mathcal{GGIW}(\mathbf{y}_k; \zeta_{j,i_C,k}^{c,\mathbf{C}_c}) \qquad \text{(A32)} \end{aligned}$$

and the likelihood $\mathcal{L}_{\mathbf{C}_c,k}^{j,i_C}$ is given by

$$\begin{aligned} \mathcal{L}_{\mathbf{C}_c,k}^{j,i_C} &= r_+^{j,i_C} \left\langle f_+^{j,i_C}(\mathbf{y}_k); \psi_{\mathbf{C}_c}(\mathbf{y}_k)\psi_{\mathbf{Z}_k^{p,c}}(\mathbf{y}_k) \right\rangle \\ &= r_+^{j,i_C} \sum_{c=1}^{n_c} \mu_{j,i_C,k|k-1}^c Q_k^{c,\mathbf{C}_c} G_k^{c,\mathbf{C}_c} \Delta_k^{c,\mathbf{C}_c} \end{aligned} \tag{A33}$$

Similarly, given the predicted PPP intensity,

$$D_+^u(\mathbf{y}_k) = \mu_{D^u,k|k-1}^c \sum_{n=1}^{J_{u,k|k-1}} w_{u,k|k-1}^{c,n} \mathcal{GGIW}(\mathbf{y}_k; \zeta_{u,k|k-1}^{c,n}) \tag{A34}$$

the updated density for the first detection target is given by

$$\begin{aligned} f_{\mathbf{C}_c}^u(\mathbf{y}_k|\mathbf{Z}^k) &= \frac{\psi_{\mathbf{C}_c}(\mathbf{y}_k)\psi_{\mathbf{Z}_k^{p,c}}(\mathbf{y}_k) D_+^u(\mathbf{y}_k)}{\left\langle D_+^u(\mathbf{y}_k); \psi_{\mathbf{C}_c}(\mathbf{y}_k)\psi_{\mathbf{Z}_k^{p,c}}(\mathbf{y}_k) \right\rangle} \\ &= \mu_{D^u,k}^{c,\mathbf{C}_c} \sum_{n=1}^{J_{u,k|k-1}} w_{u,k}^{c,\mathbf{C}_c,n} \mathcal{GGIW}(\mathbf{y}_k; \zeta_{u,k}^{c,\mathbf{C}_c,n}) \end{aligned} \tag{A35}$$

where

$$\mu_{D^u,k}^{c,\mathbf{C}_c} = \frac{\mu_{D^u,k|k-1}^c \sum_{n=1}^{J_{u,k|k-1}} w_{u,k|k-1}^{c,n} Q_k^{c,\mathbf{C}_c,n} G_k^{c,\mathbf{C}_c,n} \Delta_k^{c,\mathbf{C}_c,n}}{\sum_{c=1}^{n_c} \mu_{D^u,k|k-1}^c \sum_{n=1}^{J_{u,k|k-1}} w_{u,k|k-1}^{c,n} Q_k^{c,\mathbf{C}_c,n} G_k^{c,\mathbf{C}_c,n} \Delta_k^{c,\mathbf{C}_c,n}} \tag{A36}$$

$$w_{u,k}^{c,\mathbf{C}_c,n} = \frac{w_{u,k|k-1}^{c,n} Q_k^{c,\mathbf{C}_c,n} G_k^{c,\mathbf{C}_c,n} \Delta_k^{c,\mathbf{C}_c,n}}{\sum_{n=1}^{J_{u,k|k-1}} w_{u,k|k-1}^{c,n} Q_k^{c,\mathbf{C}_c,n} G_k^{c,\mathbf{C}_c,n} \Delta_k^{c,\mathbf{C}_c,n}} \tag{A37}$$

$$\mathcal{L}_{\mathbf{C}_c,k}^{u} = \sum_{c=1}^{n_c} \mu_{D^u,k|k-1}^{c} \sum_{n=1}^{J_{u,k|k-1}} w_{u,k|k-1}^{c,n} Q_k^{c,\mathbf{C}_c,n} G_k^{c,\mathbf{C}_c,n} \Delta_k^{c,\mathbf{C}_c,n} \tag{A38}$$

References

1. Paul, M.M.; Sergiu, N.; Radu, D. Robust Data Association Using Fusion of Data-Driven and Engineered Features for Real-Time Pedestrian Tracking in Thermal Images. *Sensors* **2021**, *21*, 8005. [CrossRef]
2. Mahler, R. *Statistical Multisource-Multitarget Information Fusion*; Artech House: Norwood, MA, USA, 2007.
3. Bar-Shalom, Y.; Kumar, A.; Blair, W.D.; Groves, G.W. Tracking low elevation targets in the presence of multipath propagation. *IEEE Trans. Aerosp. Electron. Syst.* **1994**, *30*, 973–979. [CrossRef]
4. Angle, R.B.; Streit, R.L.; Efe, M. Multiple Target Tracking With Unresolved Measurements. *IEEE Signal Process. Lett.* **2021**, *28*, 319–323. [CrossRef]
5. Gilholm, K.; Godsill, S.; Maskell, S.; Salmond, D. Poisson models for extended target and group tracking. *Signal Data Process. Small Targets* **2005**, *5913*, 59130R. [CrossRef]
6. Feldmann, M.; Franken, D.; Koch, W. Tracking of extended objects and group targets using random matrices. *IEEE Trans. Signal Process.* **2011**, *59*, 1409–1420. [CrossRef]
7. Lan, J.; Li, X.R. Tracking of extended object or target group using random matrix: New model and approach. *IEEE Trans. Aerosp. Electron. Syst.* **2016**, *52*, 2973–2989. [CrossRef]
8. Richter, T.; Seiler, J.; Schnurrer, W.; Kaup, A. Robust super-resolution for mixed-resolution multiview image plus depth data. *IEEE TRansactions Circuits Syst. Video Technol.* **2016**, *26*, 814–828. [CrossRef]
9. Liu, A.; Wang, F.; Xu, H.; Li, L. N-SAR: A new multichannel multimode polarimetric airborne SAR. *IEEE J. Sel. Top. Appl. Earth Observations Remote. Sens.* **2018**, *11*, 3155–3166. [CrossRef]
10. Granström, K.; Lundquist, C.; Orguner, U. Tracking rectangular and elliptical extended targets using laser measurements. In Proceedings of the International Conference Information Fusion, Chicago, IL, USA, 5–8 July 2011; pp. 1–8.
11. Aftab, W.; Hostettler, R.; Freitas, A.D.; Arvaneh, M.; Mihaylova, L. Spatio-temporal Gaussian process models for extended and group object tracking with irregular shapes. *IEEE Trans. Veh. Technol.* **2019**, *68*, 2137–2151. [CrossRef]
12. Gao, L.; Battistelli, G.; Chisci, L.; Farina, A. Fusion-Based Multidetection Multitarget Tracking With Random Finite Sets. *IEEE Trans. Aerosp. Electron. Syst.* **2021**, *57*, 2438–2458. [CrossRef]
13. Gao, L.; Battistelli, G.; Chisci, L. PHD-SLAM 2.0: Efficient SLAM in the Presence of Missdetections and Clutter. *IEEE Trans. Robot.* **2021**, *37*, 1834–1843. [CrossRef]
14. Gao, L.; Battistelli, G.; Chisci, L. Fusion of Labeled RFS Densities With Minimum Information Loss. *IEEE Trans. Signal Process.* **2020**, *68*, 5855–5868. [CrossRef]
15. Gao, L.; Sun, W.; Wei, P. Extensions of the CBMeMBer filter for joint detection, tracking, and classification of multiple maneuvering targets. *Digit. Signal Process.* **2016**, *56*, 35–42. [CrossRef]
16. Florian, T.; Shishan, Y.; Marcus, B. GM-PHD filter for multiple extended object tracking based on the multiplicative error shape model and network flow labeling. In Proceedings of the IEEE Intelligent Vehicles Symposium (IV), Los Angeles, CA, USA, 11–14 June 2017; pp. 7–12.
17. Granstrom, K.; Orguner, U. A PHD filter for tracking multiple extended targets using random matrices. *IEEE Trans. Signal Process.* **2012**, *60*, 5657–5671. [CrossRef]
18. Granstrom, K.; Orguner, U. Estimation and maintenance of measurement rates for multiple extended target tracking. In Proceedings of the International Conference Information Fusion, Singapore, 9–12 July 2012; pp. 2170–2176.
19. Baum, M.; Hanebeck, U.D. Extended object tracking with random hypersurface models. *IEEE Trans. Aerosp. Electron. Syst.* **2014**, *50*, 149–159. [CrossRef]
20. Wahlström, N.; Özkan, E. Extended target tracking using Gaussian processes. *IEEE Trans. Signal Process.* **2015**, *63*, 4165–4178. [CrossRef]
21. Nil, G.; Alessio, F.; Angelo, C.; Henk, W.; Canan, A.; Rico, M.; Gonzalo, S. Cramér-Rao Bound analysis of Radars for extended vehicular targets with known and unknown shape. *IEEE Trans. Signal Process.* **2022**, *70*, 3280–3295. [CrossRef]
22. Cao, X.; Lan, J.; Rong Li, X. Extension-Deformation approach to extended object tracking. *IEEE Trans. Aerosp. Electron. Syst.* **2021**, *57*, 866–881. [CrossRef]
23. Mahler, R. PHD filters for nonstandard targets, I: Extended targets. In Proceedings of the International Conference Information Fusion, Seattle, WA, USA, 6–9 July 2009; pp. 915–921.
24. Vo, B.; Ma, W. The Gaussian mixture probability hypothesis density filter. *IEEE Trans. Signal Process.* **2006**, *54*, 4091–4104. [CrossRef]

25. Viktor, E.; Maria, A.; Granström, K.; Fredrik, G. Pedestrian group tracking using the GM-PHD filter. In Proceedings of the 21st European Signal Processing Conference (EUSIPCO 2013), Marrakech, Morocco, 9–13 September 2013; pp. 1–5.
26. Lundquist, C.; Granström, K.; Orguner, U. An extended target CPHD filter and a gamma Gaussian inverse Wishart implementation. *IEEE J. Sel. Top Signal Process.* **2013**, *7*, 472–483. [CrossRef]
27. Zhang, G.; Lian, F.; Han, C. CBMeMBer filters for nonstandard targets, I: Extended targets. In Proceedings of the International Conference Information Fusion, Salamanca, Spain, 7–10 July 2014; pp. 1–6.
28. Hu, Q.; Ji, H.; Zhang, Y. Tracking multiple extended targets with multi-Bernoulli filter. *IET Signal Process.* **2019**, *13*, 443–455. [CrossRef]
29. Beard, M.; Reuter, S.; Granström, K.; Vo, B.; Vo, B.; Scheel, A. Multiple extended target tracking with labeled random finite sets.*IEEE Trans. Signal Process.* **2016**, *64*, 1638–1653. [CrossRef]
30. Beard, M.; Reuter, S.; Granström, K.; Vo, B.-T.; Vo, B.-N.; Scheel, A. A generalised labelled multi-Bernoulli filter for extended multi-target tracking. In Proceedings of the International Conference Information Fusion, Washington, DC, USA, 6–9 July 2015; pp. 991–998.
31. Fernández, F.; Williams, J.L.; Granström, K.; Svensson, L. Poisson multi-bernoulli mixture filter: Direct derivation and implementation. *IEEE Trans. Aerosp. Electron. Syst.* **2018**, *54*, 1883–1901. [CrossRef]
32. Granström, K.; Fatemi, M.; Svensson, L. Poisson multi-Bernoulli mixture conjugate prior for multiple extended target filtering. *IEEE Trans. Aerosp. Electron. Syst.* **2020**, *56*, 208–225. [CrossRef]
33. Williams, J.L. Marginal multi-Bernoulli filters: RFS derivation of MHT, JIPDA, and association-based member. *IEEE Trans. Aerosp. Electron. Syst.* **2015**, *51*, 1664–1687. [CrossRef]
34. Granström, K.; Fatemi, M.; Svensson, L. Gamma gaussian inverse-wishart poisson multi-Bernoulli filter for extended target tracking. In Proceedings of the International Conference Information Fusion, Heidelberg, Germany, 5–8 July 2016; pp. 893–900.
35. Li, Y.; Wei, P.; Li, G.; Chen, Y.; Gao, L.; Zhang, H. Joint detection, tracking and classification of multiple extended objects based on the JDTC-GIW-MeMBer filter. *Signal Process.* **2021**, *178*, 107800. [CrossRef]
36. Hu, Q.; Ji, H.; Zhang, Y. A standard PHD filter for joint tracking and classification of maneuvering extended targets using random matrix. *Signal Process.* **2018**, *144*, 352–363. [CrossRef]
37. Sun, L.; Lan, J.; Li, X.R. Joint tracking and classification of extended object based on support functions. *IET Radar Sonar Navig.* **2018**, *12*, 685–693. [CrossRef]
38. Yang, W.; Wang, Z.; Fu, Y.; Pan, X.; Li, X. Joint detection, tracking and classification of a manoeuvring target in the finite set statistics framework. *IET Signal Process.* **2015**, *9*, 10–20. [CrossRef]
39. Dan, L.; Wong, K.D.; Hu, H.; Sayeed, A.M. Detection, classification, and tracking of targets. *IEEE Signal Process. Mag.* **2002**, *19*, 17–29. [CrossRef]
40. Chavez-Garcia, R.O.; Aycard, O. Multiple sensor fusion and classification for moving object detection and tracking. *IEEE Trans. Intell. Transp. Syst.* **2016**, *17*, 525–534. [CrossRef]
41. Li, Y.; Wei, P.; Wei, Y.; Gao, L.; Zhang, H. Loopy sum-product algorithm based joint detection, tracking and classification of extended objects with analytic implementations. *Signal Process.* **2022**, *196*, 108520. [CrossRef]
42. Okello, N.; Thorns, G. Threat assessment using Bayesian networks. In Proceedings of the International Conference Information Fusion, Cairns, QLD, Australia, 8–11 July 2003; pp. 1102–1109.
43. Nguyen, X.T. Threat assessment in tactical airborne environments. In Proceedings of the International Conference Information Fusion, CAnnapolis, MD, USA, 8–11 July 2002; pp. 1300–1307.
44. Jiang, H.; Xu, L.; Zhan, K. Joint tracking and classification based on aerodynamic model and radar cross section. *Pattern Recognit.* **2014**, *47*, 3096–3105. [CrossRef]
45. Xu, K.; Kong, D.; Chen, J. Target threat assessment based on improved RBF neural network. In Proceedings of the Chinese Intelligent Automation Conference, Fuzhou, China, 30 March 2015; pp. 559–566. [CrossRef]
46. Lan, J.; Li, X. Joint tracking and classification of extended object using random matrix. In Proceedings of the International Conference Information Fusion, Istanbul, Turkey, 9–12 July 2013; pp. 1550–1557.
47. Granström, K.; Svensson, L.; Reuter, S.; Xia, Y.; Fatemi, M. Likelihood-based data association for extended object tracking using sampling methods. *IEEE Trans. Intell. Veh.* **2018**, *3*, 30–45. [CrossRef]
48. Scheel, A.; Granström, K.; Meissner, D.; Reuter, S.; Dietmayer, K. Tracking and data segmentation using a GGIW filter with mixture clustering. In Proceedings of the International Conference Information Fusion, Salamanca, Spain, 7–10 July 2014; pp. 1–8.
49. Bar-Shalom, Y. *Multitarget-Multisensor Tracking: Applications and Advances*; Artech House: Norwood, MA, USA, 2000; Volume 3.
50. Granström, K.; Lundquist, C.; Orguner, O. Extended target tracking using a Gaussian-mixture PHD filter. *IEEE Trans. Aerosp. Electron. Syst.* **2012**, *48*, 3268–3286. [CrossRef]
51. Schuhmacher, D.; Vo, B.; Vo, B. A consistent metric for performance evaluation of multi-object filters. *IEEE Trans. Signal Process.* **2008**, *56*, 3447–3457. [CrossRef]
52. Li, X.R.; Jilkov, V.P. Survey of maneuvering target tracking. Part V. Multiple-model methods. *IEEE Trans. Aerosp. Electron. Syst.* **2005**, *41*, 1255–1321. [CrossRef]

53. Murty, K. An algorithm for ranking all the assignments in order of increasing cost. *Oper. Res.* **1968**, *16*, 682–687. [CrossRef]
54. Williams, J.L. An efficient, variational approximation of the best fitting multi-Bernoulli filter. *IEEE Trans. Signal Process.* **2015**, *63*, 258–273. [CrossRef]